Howie Choset

Carnegie Mellon University
Scaife Hall
Pittsburgh, Pennsylvania 15213 USA
choset@cs.cmu.edu

Joel Burdick

California Institute of Technology
Mail Code 104-44
Pasadena, California 91125 USA

Sensor-Based Exploration: The Hierarchical Generalized Voronoi Graph

Abstract

The hierarchical generalized Voronoi graph (HGVG) is a new roadmap developed for sensor-based exploration in unknown environments. This paper defines the HGVG structure: a robot can plan a path between two locations in its work space or configuration space by simply planning a path onto the HGVG, then along the HGVG, and finally from the HGVG to the goal. Since the bulk of the path planning occurs on the one-dimensional HGVG, motion planning in arbitrary dimensioned spaces is virtually reduced to a one-dimensional search problem. A bulk of this paper is dedicated to ensuring the HGVG is sufficient for motion planning by demonstrating the HGVG (with its links) is an arc-wise connected structure. All of the proofs in this paper that lead toward the connectivity result focus on a large subset of spaces in $\mathbb{R}^3$, but wherever possible, results are derived in $\mathbb{R}^m$. In fact, under a strict set of conditions, the HGVG (the GVG by itself) is indeed connected, and hence sufficient for motion planning. The chief advantage of the HGVG is that it possesses an incremental construction procedure, described in a companion paper, that constructs the HGVG using only line-of-sight sensor data. Once the robot constructs the HGVG, it has effectively explored the environment, because it can then use the HGVG to plan a path between two arbitrary configurations.

KEY WORDS—sensor-based exploration, skeletons, roadmap, Voronoi diagrams, motion planning

1. Introduction

This work addresses two canonical sensor-based motion-planning problems for a robot without prior information about an environment: (1) find a collision-free path to a goal and (2) map a bounded environment with a systematic exploration procedure. Since in a bounded environment, the solution to the mapping problem automatically solves the collision-free path-planning problem, we will focus attention on the geometric structure necessary for exploration.

Our mapping procedure relies on a *roadmap*, a network of one-dimensional curves that concisely represents the salient geometry of a robot's environment. A planner can construct a path between any two points in a connected component of the robot's free space by finding a path onto the roadmap, traversing the roadmap to the vicinity of the goal, and constructing a path from the roadmap to the goal.

This paper introduces a new roadmap termed the *hierarchical generalized Voronoi graph* (HGVG), which can be incrementally constructed using only line-of-sight sensor data. An incremental construction procedure is important because most environments do not have a single vantage point from which the robot can "see" everything, and thus the robot must systematically move around the environment. Once the robot has incrementally constructed the roadmap for an environment, it has in essence explored the environment. The HGVG incremental construction procedure is described in the companion paper (Choset et al. 2000).

The HGVG is defined in terms of line-of-sight distance measurements, information that sensors can provide. Most sensor-based motion planners are limited to planar configuration spaces, but the HGVG is also useful in multidimensional spaces where the bulk of the motion planning still occurs in a one-dimensional search space. The HGVG approach differs from other sensor-based planners in that it offers completeness guarantees that ensure the robot can find a path from start to goal or report that such a path is not feasible.

While sensor-based planning motivates this work, the HGVG has many other applications when full knowledge of the world is available. Potential application areas include CAD modeling, injection molding, visibility planning, and inspection. For example, just as the HGVG reveals the

underlying geometry of a robot's environment, it could also emit the geometry of an injection mold. A designer could infer mold properties from the HGVG, early in the design phase, before committing to a particular design.

1.1. Relation to Prior Work

Robotic *motion planning* generally determines a *path* that a robot must follow to reach a goal location or configuration without penetrating any obstacles (Latombe 1991). This path may exist in the robot's environment or in the robot's *configuration space,* the set of all robot locations and postures that do not intersect an obstacle for a particular environment. A motion planner is *complete* if it can, in finite time, find a path or determine that no such path exists.

Classical motion planning assumes that the robot has a priori information about the environment, but when the robot does not have any previous information, it must rely on sensor information. Therefore, the robot must use *sensor-based* motion planning. This type of planning has recently received increased attention, as it is a requirement for the realistic deployment of autonomous robots into unstructured and completely unknown environments.

Much current work in sensor-based planning applies to two-dimensional scenarios and is heuristic (therefore, not complete). One class of heuristic algorithms employs a behavioral-based approach, in which the robot is armed with a simple set of behaviors (e.g., following a wall) (Brooks 1986). A hierarchy of cooperating behaviors then composes more complicated actions, such as exploration. Sequencing constitutes an extension of this approach (Gat and Dorais 1994). While strong experimental results suggest the utility of the behavioral approaches, none of these methods possesses proofs of correctness guaranteeing that a path can be found, nor do they contain well-established thresholds specifying when their heuristic algorithms fail. Finally, these approaches do not generalize to higher dimensions.

Complete sensor-based planners are typically limited to the plane (Rao et al. 1993). For example, one of the first complete sensor-based schemes is Lumelsky's "bug" algorithm (Lumelsky and Stepanov 1987), but it is limited to the plane and does not provide a map of the environment. One of the first complete sensor-based schemes to map an unknown environment is described in Rao, Stolzfus, and Iyengar (1991). This method is based on the generalized Voronoi diagram, described below, and is also limited to the plane.

Our approach adapts the structure of a rigorous motion-planning scheme that functions in higher dimensions. One such method relies on a *roadmap* (Canny 1988), a concept analogous to highway systems having the following properties of *accessibility*, *connectivity*, and *departability*. Accessibility means that the planner can construct a path from any point in the environment onto the roadmap. Connectivity, as its name suggests, means that the roadmap is connected, i.e.,

there is only one connected roadmap per connected region of free space. Finally, departability means that a path can be constructed from a point on the roadmap to any point in the free space.

An example of a roadmap scheme is the Opportunistic Path Planner (OPP) (Canny and Lin 1993). Rimon adapted this motion-planning scheme for sensor-based use (Rimon and Canny 1994). The sensor-based planner requires active perception to guarantee connectivity of the roadmap, but it does not describe the active perception procedure nor when to invoke it. Furthermore, the sensor-based approach does not contain a detailed procedure for constructing the roadmap fragments from sensor data, and finally, the robot must contain sensors that can detect "interesting critical points" and "interesting saddle points," whose implementation is described only for a handful of special cases.

Another type of roadmap is the *generalized Voronoi diagram* (GVD), the locus of points equidistant to two or more obstacles. The GVD is an extension of the Voronoi diagram (VD), the set of points equidistant to two or more points (sometimes termed sites) in the plane. The GVD was first used almost 20 years ago in robotics for machine vision (Rowat 1979). Active research in applying the GVD to motion planning began with Ó'Dúnlaing and Yap 1985), who considered motion planning for a disk in the plane. However, their method requires full knowledge of the world's geometry prior to the planning event and its retract methodology may not extend to nonplanar problems. Later work (Rao, Stolzfus, and Iyengar 1991) introduces an incremental approach to create a GVD-like structure, which is limited to the case of a plane. Prior work (Avis and Bhattacharya 1983) describes the *Voronoi graph* (VG), which is the one-dimensional locus of points in m dimensions equidistant to m point sites. Our approach can be viewed as a blend of the OPP and Voronoi methods.

1.2. Contributions

The HGVG roadmap represents one of the first motion-planning techniques that (1) relies only on line-of-sight sensor information, (2) functions in higher dimensions, and (3) offers completeness guarantees. Since many sensors provide distance information, a motion planner that relies on a distance function, one that measures the distance between a point and an obstacle, is useful for sensor-based planning. The GVD roadmap is well suited to sensor-based implementation because it is defined in terms of just such function.

Nevertheless, to accommodate free-flying and highly articulated robots, the challenge is to develop a roadmap for multidimensional spaces. The GVD is only a roadmap for planar environments. Consequently, the first step in this work produces the *generalized Voronoi graph* (GVG), which is a natural extension of the GVD into higher dimensions; it is the one-dimensional set of points in m dimensions equidistant to m obstacles.

However, unlike the GVD, the GVG is not necessarily connected in dimensions greater than two, and thus, in general, is not a roadmap. Additional structures, termed *higher order generalized Voronoi graphs*, connect GVG components, and together with the GVG form the HGVG. The HGVG is well suited to motion planning in multidimensional spaces (such as configuration spaces) because a motion planner can perform a bulk of its search on the one-dimensional HGVG. Figure 1 summarizes the evolution of the HGVG.

1.3. Basic Assumptions

Throughout this work, we assume that the robot is modeled as a point operating in a subset $\mathcal{W}$ of an m-dimensional Euclidean space. We term $\mathcal{W}$ to be the work space even though it could be the robot's work space or configuration space, which is C^2-diffeomorphic to $\mathbb{R}^m$. The work space $\mathcal{W}$ is populated by obstacles $C_1, \ldots, C_n$, which are closed sets. We assume, when necessary, that nonconvex obstacles are locally convex, i.e., they are modeled as the union of the convex sets. For example, in Figure 2, the robot considers the L-shaped obstacle as two obstacles when attending to the "interior" of the L, but as one when focusing on the regions: the left and underneath the L. This makes sense from a sensor-based point of view. When the robot is "in" the L, it "sees" two objects that connect, whereas outside and to the left, the robot "sees" one obstacle. The set of points where the robot is free to move is called the *free space* and is defined as $\mathcal{FS} = \mathcal{W}\backslash \bigcup_{i=1}^{i=n} C_i$ (see Fig. 2).

This work makes two assumptions underlying the placement of obstacles in the environment. The first is stated below, and the second is introduced in Section 3.4. Finally, for $x \in \mathbb{R}^m$, let nbhd(x) be a neighborhood of x that is contained in $\mathbb{R}^m$.
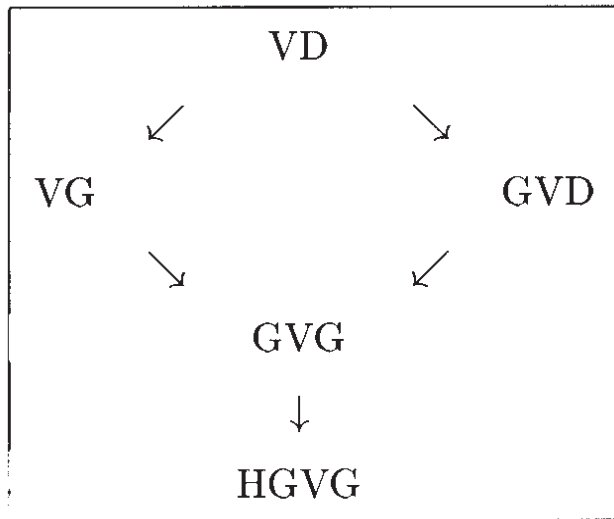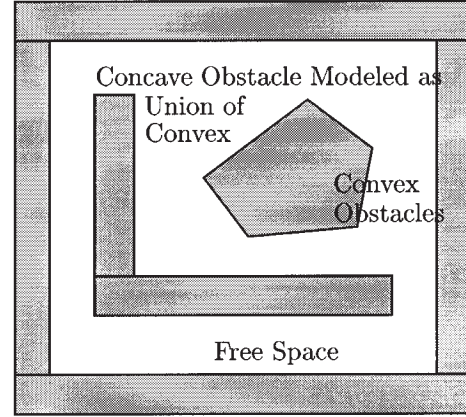

Fig. 1. Evolution of the HGVG.

Fig. 2. The robot operates in a bounded subset of the free space. Concave obstacles are modeled as the union of convex obstacles.

ASSUMPTION 1.   Boundedness Assumption: The robot operates in a bounded, connected subset of the free space $\mathcal{FS}$. This subset is bounded by obstacles.

When Assumption 1 is valid, $n \geq m + 1$. For example, in $\mathbb{R}^3$ it takes a minimum four convex obstacles to bound a subset of $\mathcal{FS}$. Also note that when Assumption 1 holds, although the robot is operating in a bounded connected subset of $\mathcal{FS}$, the free space $\mathcal{FS}$ itself may be unbounded.

2. Distance Functions

The HGVG is defined in terms of a distance function that measures distance between a point and an obstacle. This section defines two types of distance functions: the X-distance function and the V-distance function, both of which provide a geometric foundation for our definition of the roadmap. A more complete discussion of these functions and their properties can be found in Choset and Burdick (1994).

2.1. X-Distance Function

The distance between a point x and a convex set C_i is

$$d_i^X(x) = \min_{c_0 \in C_i} \|x - c_0\|, \tag{1}$$

where $\| \cdot \|$ is the two-norm in $\mathbb{R}^m$. In Clarke (1990), it is shown that the gradient of $d_i^X(x)$ is

$$\nabla d_i^X(x) = \frac{x - c_0}{\|x - c_0\|} \in T_x\mathbb{R}^m, \tag{2}$$

where c_0 is the point closest to x in C_i. That is, c_0 is the point where $\|x - c_0\| = \min_{c \in C_i} \|x - c\|$. In later sections, we write $c_0 = \text{argmin} d_i^X(x)$. The gradient $\nabla d_i^X(x)$ is a unit vector, based at x, pointing away from c_0 along a line defined

by c_0 and x (see Fig. 3). For convex sets, the closest point is always unique and thus, in the interior of the free space, the single object distance function is smooth (Clarke 1990).

Typically, the environment is populated with multiple obstacles, and thus we define a *multiobject distance function*, which is the distance between a point x and the closest point in the closest obstacle, i.e.,

$$D(x) = \min_i d_i^X(x). \tag{3}$$

Sometimes, $D(x)$ can be stated as the distance between a point and the environment.

The multiobject distance function is nonsmooth (Choset 1998), and hence its gradient cannot be trivially defined. However, using nonsmooth analysis, which is reviewed in Choset (1998), it can be shown that the *generalized gradient* of $D(x)$ is

$$\partial D(x) = \text{Co}\{\nabla d_i^X(x) \: : \: i \in I(x)\}, \tag{4}$$

where (1) Co is the convex hull operation, (2) ∂ is the generalized gradient operator, and (3) $I(x)$ is defined as the set of indices such that $\forall i \in I(x)$, each C_i is the closest object to x (x may be equidistant to two or more obstacles). Notationally, if ∂ appears in front of a set, as opposed to a function, then it refers to the boundary of the set.

The definition of the distance function in this section does not consider occlusions. That is, the distance between a point x and an obstacle C_i can always be determined, even if there are other obstacles between x and C_i. Therefore, for the sake of terminology, we will term the particular distance function defined in this section as the *X-distance function* because its implementation assumes a robot can see through obstacles, as if the robot has X-ray vision.
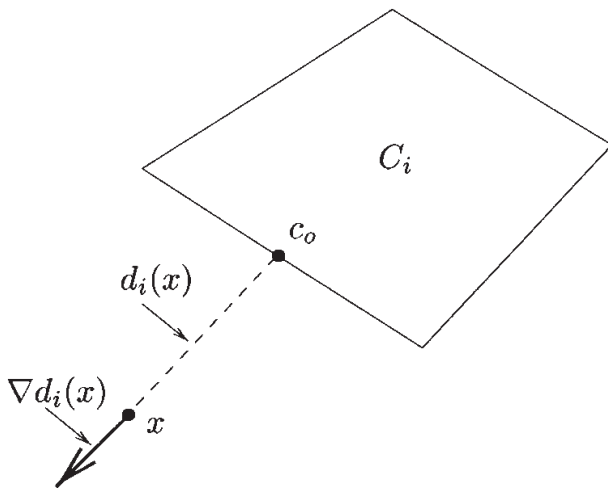
2.2. The V-Distance Function

Since most robot sensors cannot see through obstacles, we will now develop a distance function that relies solely on line-of-sight measurements. First, we consider line of sight between two points, and then between a point and an obstacle. A point c is *within line of sight* of a point x if there exists a straight line segment that connects x and c without penetrating any obstacle. That is, c is within line of sight of x if for all $t \in [0, 1]$, $(x(1 - t) + ct)$ lies in $\mathcal{FS}$.

Now consider line of sight between a point and an obstacle. Let $\tilde{C}_i(x)$ be the set of points on an object C_i that are within line of sight of x, i.e.,

$$\tilde{C}_i(x) = \{c \in C_i \: : \: (1 - t)x + ct \in \mathcal{FS}, \; \forall t \in [0, 1]\}.$$

Let c be the nearest point in C_i to x, as defined by the X-distance function, i.e., $c = \text{argmin} d_i^X(x)$. The obstacle C_i is *within visible line of sight* at a point x, if the line segment that connects c and x does not penetrate any other obstacle. In other words, C_i is within visible line of sight at x if $c \in \tilde{C}_i(x)$. In Figure 4, the nearest points on objects C_j and C_k, as measured by the X-ray distance function, are within line of sight of x and hence C_j and C_k are within visible line of sight of x.

If $\tilde{C}_i(x) = \emptyset$, then C_i is *fully occluded* at x. In other words, there are no points on the object that are within line of sight of x. Finally, there is an intermediate notion occlusion. If $c \notin \tilde{C}_i(x)$, the obstacle is *visibly occluded* at x. In Figure 4, the nearest point on object C_i, as measured by the X-ray distance function, is *not* within line of sight of x, and hence it is not within visible line of sight of x, i.e., C_i is visibly occluded at x. With this notion of visible line of sight, we can define distance as

DEFINITION 1. The *V-distance function* measures the distance between a point x and visible line-of-sight obstacle C_i, as the distance between x and the closest point on C_i to x. If

Fig. 3. Distance between x and C_i is the distance to the closest point on C_i. The gradient is a unit vector pointing away from the nearest point.
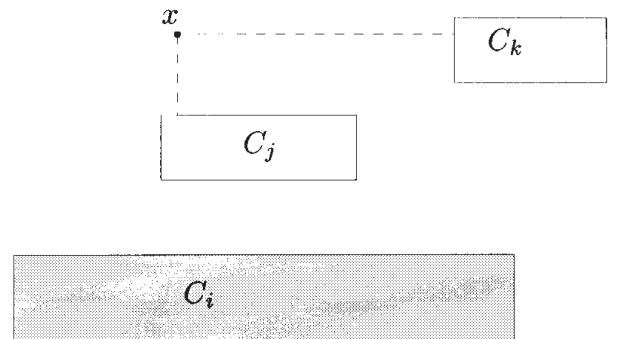

Fig. 4. Using the V-distance function, the distance to C_i is infinity, i.e., C_i is visibly occluded.

C_i is not within visible line of sight at x, then the distance is infinity, i.e., let $c = \mathrm{argmin} d_i^X(x)$, and

$$d_i^V(x) = \begin{cases} \min_{c \in C_i} \|x - c\|, & \text{if } c \in \mathrm{interior}(\tilde{C}_i(x)), \\ \infty, & \text{if } c \notin \mathrm{interior}(\tilde{C}_i(x)), \end{cases}$$
(5)

where interior means the interior of a set.

In Figure 4, C_i is not within visible line of sight at x, and thus it is occluded at x, making C_k the second closest obstacle.

If an object is not occluded, then the distance function has an associated gradient, i.e., letting $c = \mathrm{argmin} d_i^X(x)$, we have

$$\nabla d_i^V(x) = \begin{cases} \frac{x-c}{\|x-c\|} & \text{if } c \in \mathrm{interior}(\tilde{C}_i(x)), \\ \text{undefined}, & \text{if } c \notin \mathrm{interior}(\tilde{C}_i(x)). \end{cases}$$
(6)

By definition, $D(x) = \min_i d_i^V(x) = \min_i d_i^X(x)$. Throughout this work, we will use the visible distance function, so the V-superscript is omitted.

Since this distance function is based only on line-of-sight information, it is more conducive to implementation with realistic sensors than the X-distance function. In fact, an important characteristic of $d_i(x)$ and $\nabla d_i(x)$ is that they can be computed from sensor data. For example, consider a mobile robot with a ring of sonar sensors (Fig. 5). The sonar sensor measurement approximates the value of the distance function, and the direction opposite to which the sensor is facing approximates the distance gradient.

3. The Generalized Voronoi Graph

The distance function provides the basis for the HGVG and related structures such as the GVG and GVD. In this section,
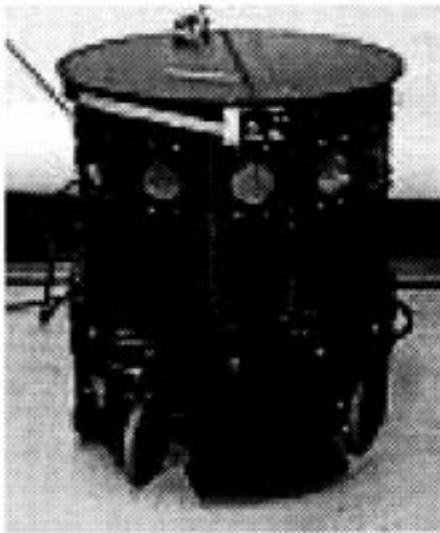

Fig. 5. Mobile robot with sonar ring.

we describe the structures that comprise the GVG and then show that the GVG is one-dimensional. To do this, we must introduce a stability assumption requiring that obstacles lie in a generic environment. Finally, we will discuss the properties of accessibility and connectivity.

3.1. Equidistant Faces

In the Voronoi diagram literature, a *Voronoi region* is the set of points closest to a particular site (Aurenhammer 1991). Here, this definition is extended to the *generalized Voronoi region*, $\mathcal{F}_i$, which is the closure of the set of points closest to one particular obstacle. In other words,

$$\mathcal{F}_i = \mathrm{cl}\{x \in \mathcal{FS} : d_i(x) \le d_h(x) \ \ \forall h \ne i\}. \quad (7)$$

The basic building block of the GVD and GVG is the set of points equidistant to two sets C_i and C_j, which we term the *two-equidistant surface*,

$$\mathcal{S}_{ij} = \{x \in \mathcal{W} \backslash (C_i \textstyle\bigcup C_j) : d_i(x) - d_j(x) = 0\}.$$

See Figure 6. Of particular interest is the subset of $\mathcal{S}_{ij}$ termed the *two-equidistant surjective surface*,

$$\mathcal{SS}_{ij} = \mathrm{cl}\{x \in \mathcal{S}_{ij} : \nabla d_i(x) \ne \nabla d_j(x)\}, \quad (8)$$

which is the set of points x equidistant to two objects such that $\nabla d_i(x) \ne \nabla d_j(x)$, i.e., the function $\nabla (d_i - d_j)(x)$ is surjective for all $x \in \mathcal{SS}_{ij}$. Algebraically, this definition satisfies some requirements of the preimage theorem (Abraham, Marsden, and Ratiu 1988), but in actuality, the definition of $\mathcal{SS}_{ij}$ accommodates nonconvex sets (see Fig. 7). If C_i and C_j are disjoint convex obstacles, then $\mathcal{SS}_{ij} = \mathcal{S}_{ij}$. We are interested in yet a further subset of $\mathcal{SS}_{ij}$, which is

DEFINITION 2. The *two-equidistant face* is the set of points equidistant to obstacles C_i and C_j, such that each point x in $\mathcal{F}_{ij}$ is closer to C_i and C_j than to any other obstacle, i.e.,

$$\mathcal{F}_{ij} = \{x \in \mathrm{cl}(\mathcal{SS}_{ij}) : d_i(x) = d_j(x) \le d_h(x) \quad \forall h \ne i, j\}. \quad (9)$$

By definition, $\mathcal{F}_{ij} \subset \mathrm{cl}(\mathcal{FS})$. Note that a two-equidistant $\mathcal{F}_{ij}$ lies on the common boundary of adjacent generalized Voronoi regions, $\mathcal{F}_i$ and $\mathcal{F}_j$, i.e., $\mathcal{F}_{ij} = \mathcal{F}_i \bigcap \mathcal{F}_j$. See Figure 8 for an example of $\mathcal{F}_{ij}$.

The union of all two-equidistant faces forms the generalized Voronoi diagram, i.e., GVD $= \bigcup_{i=1}^{n-1} \bigcup_{j=i+1}^{n} \mathcal{F}_{ij}$ (see Fig. 9). Note that the GVD can be thought of as a complex that separates a space into generalized Voronoi regions — regions closest to a particular obstacle.

The GVD reduces the motion-planning problem by one dimension, but that is not sufficient. Consider a 30-degree-of-freedom snake robot. In $\mathbb{R}^{30}$, for example, the GVD is 29-dimensional, which still presents a complicated motion-planning problem. We seek a one-dimensional roadmap.
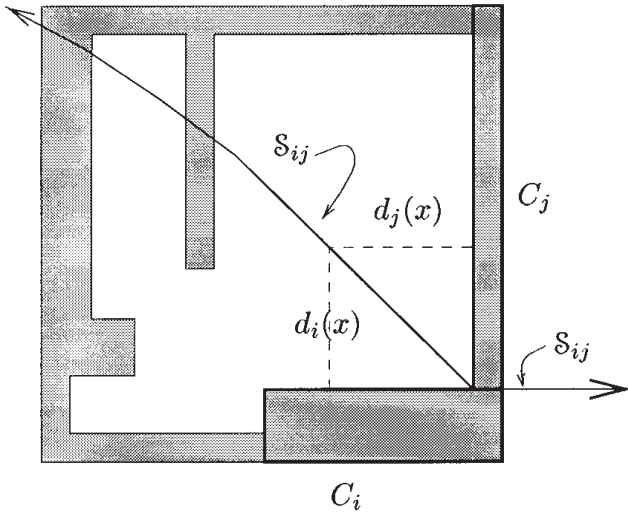
Fig. 6. The solid line represents S_{ij}, the set of points equidistant to obstacles C_i and C_j. Note that S_{ij} is unbounded and contains two components: the left component contains two linear subcomponents and one parabolic subcomponent, and the right component is linear. For all points, x, in the right component, $\nabla d_i(x) = \nabla d_j(x)$. The dotted lines emphasize that at a point on S_{ij}, $d_i(x) = d_j(x)$.
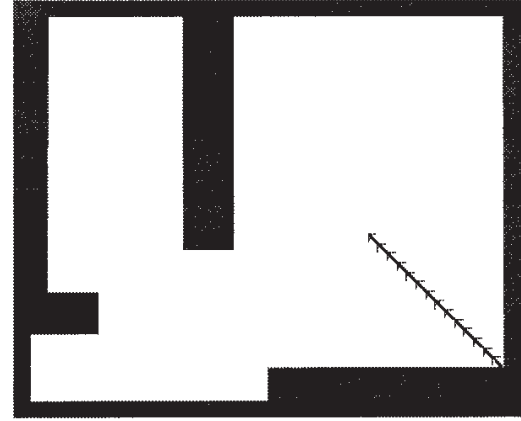

Fig. 8. The solid line with angled ticks is the set of points equidistant and closest to obstacles C_i and C_j.

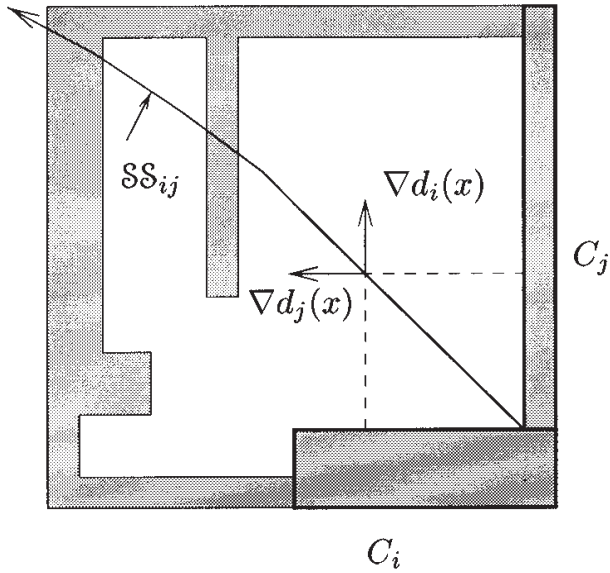Fig. 7. The thick solid line with the gentle bend represents SS_{ij}, the set of points equidistant to obstacles C_i and C_j such that the two closest points are distinct. Note that it is also unbounded and only has one connected component, unlike S_{ij}. Again, the dotted lines emphasize that for all points on SS_{ij}, $d_i(x) = d_j(x)$ and the two vectors emphasize $\nabla d_i(x) \neq \nabla d_j(x)$.
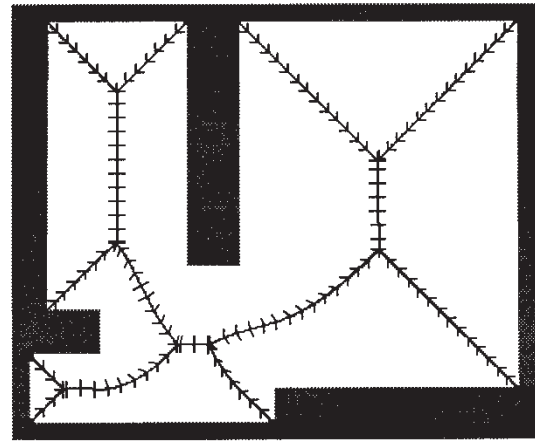

Fig. 9. The ticked solid lines is the set of points equidistant to obstacles C_i and C_j from Figure 7, such that each edge fragment is closest to the equidistant obstacles.

Therefore, to define the GVG, we continue to define lower dimensional subsets of $\mathcal{W}$. The *three-equidistant surface*, $\mathcal{S}_{ijk}$, is the set of points equidistant to three objects, C_i, C_j, and C_k, i.e., $\mathcal{S}_{ijk} = \mathcal{S}_{ij} \bigcap \mathcal{S}_{jk} \bigcap \mathcal{S}_{ik}$. Similarly, the *three-equidistant surjective surface*, $\mathcal{SS}_{ijk}$, a subset of $\mathcal{S}_{ijk}$, is the set of points equidistant to three objects, C_i, C_j, and C_k, such that for each point in $\mathcal{SS}_{ijk}$, the gradients of the individual single object distance functions are distinct, i.e., $\mathcal{SS}_{ijk} = \mathcal{SS}_{ij} \bigcap \mathcal{SS}_{jk} \bigcap \mathcal{SS}_{ik}$. The *three-equidistant face*, $\mathcal{F}_{ijk}$, a subset of $\mathcal{SS}_{ijk}$, is the set of points equidistant to C_i, C_j, and C_k, such that each point is closer to C_i, C_j, and C_k than any other obstacle, i.e.,

$$
\begin{aligned}
\mathcal{F}_{ijk} \quad &= \mathrm{cl}\{x \in \mathcal{W} : 0 \le d_i(x) = d_j(x) = d_k(x) \le d_h(x) \\
&\quad \text{such that} \quad \nabla d_i(x), \nabla d_j(x), \text{ and } \nabla d_i(x) \\
&\quad \text{are linearly independent.}\} \\
&= \mathcal{F}_{ij} \bigcap \mathcal{F}_{ik} \bigcap \mathcal{F}_{jk}.
\end{aligned}
$$

$$(10)$$

Continuing in this vein, after taking the appropriate $(k - 2)$ intersections, one can define a *k-equidistant surface*, $\mathcal{S}_{i_1 \dots i_k}$, and a *k-equidistant surjective surface*, $\mathcal{SS}_{i_1 \dots i_k}$. We rely on the Boundedness Assumption (Assumption 1) to guarantee that there exist "enough" obstacles such that $\mathcal{S}_{i_1 \dots i_k}$ and $\mathcal{SS}_{i_1 \dots i_k}$ are not empty (i.e., they exist). A subset of $\mathcal{SS}_{i_1 \dots i_k}$ of particular interest is the *k-equidistant face*, $\mathcal{F}_{i_1 \dots i_k}$, which is the set of points equidistant to objects $C_{i_1}, \dots, C_{i_k}$ such that each point is closer to objects $C_{i_1}, \dots, C_{i_k}$ than to any other object.

$$
\begin{aligned}
\mathcal{F}_{i_1 \dots i_k} &= \{x \in \mathcal{W} : 0 \le d_{i_1}(x) = \cdots = d_{i_k}(x) \le d_h(x) \text{ and } \\
&\quad \text{for all } p, q \in \{1, \dots, k\}, \ \nabla d_{i_p}(x) \ne d_{i_q}(x)\}, \\
&= \mathcal{F}_{i_1 i_2} \bigcap \mathcal{F}_{i_1 i_3} \bigcap \cdots \bigcap \mathcal{F}_{i_1 i_k}.
\end{aligned}
$$

$$(11)$$

To be consistent with the Voronoi diagram literature, in $\mathbb{R}^m$, m-equidistant faces and $(m + 1)$-equidistant faces would be termed *generalized Voronoi edges* and *generalized Voronoi vertices*, respectively. However, in this work, we term the *m-equidistant faces* as *GVG edges* and $(m + 1)$-equidistant faces as *meet points* because GVG edges meet at $(m+1)$-equidistant faces. The solid lines in Figures 10 and 11 represent GVG edges in $\mathbb{R}^3$.

3.2. Boundary Face and Floating Boundary Face

To determine the dimension of the equidistant faces, and hence the GVG edges, we must first identify the structures that lie in the boundary of equidistant faces. Observe in Figure 11 that a three-equidistant face lies in the boundary of a two-equidistant face, i.e., $\mathcal{F}_{ijk} \subset \partial \mathcal{F}_{ij}$. This can be rigorously shown via the following relationship (Choset 1996):

$$
\partial(A \bigcap B) \subset (\partial A \bigcap \mathrm{cl}(B)) \bigcup (\partial B \bigcap \mathrm{cl}(A)). \quad (12)
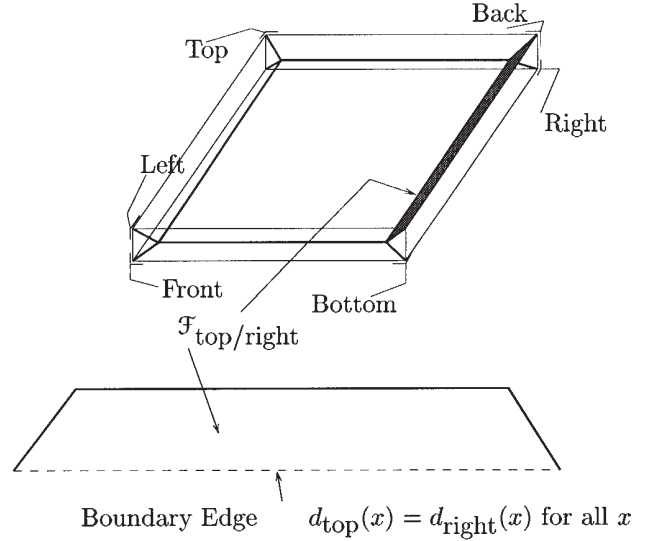$$

Fig. 10. An example of a two-equidistant face that contains a boundary edge as a portion of its boundary. The boundary edge is represented by light dotted lines, whereas the GVG edges are represented by dark solid lines.
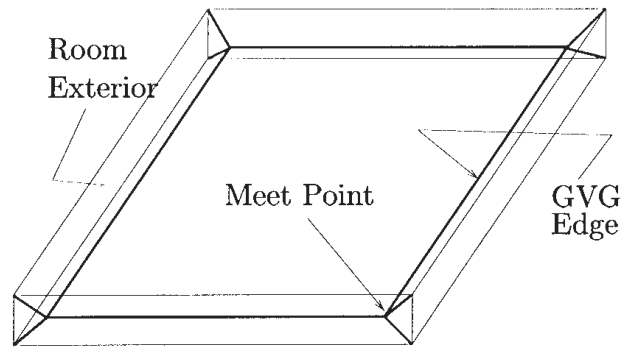

Fig. 11. The generalized Voronoi graph in a rectangular enclosure. The solid lines represent the GVG edges, which meet at vertices that are termed meet points.

Let $A = \{x : d_i(x) = d_j(x)\}$, $B = \{x : d_i(x) \geq 0\}$, and $C = \{x : \nabla d_i(x) \neq \nabla d_j(x)\}$. With these definitions,

$$
\begin{aligned}
\mathcal{F}_{ij} = \mathrm{cl}(A \bigcap B \bigcap C) = \mathrm{cl}\{x : 0 \leq d_i(x) \\
= d_j(x) \leq d_h(x) \ \forall h \text{ and } \nabla d_i(x) \neq \nabla d_j(x)\}.
\end{aligned}
\tag{13}
$$

Equation 12 implies that $\mathcal{F}_{ijk} \subset \partial\mathcal{F}_{ij}$; however, this equation also implies there are two other structures in the boundary: a two-boundary face and a floating two-boundary face, both defined below. These structures rarely occur and are not part of the GVG, but they are required in determining the appropriate dimension count for the GVG.

The set of points on the boundary of the free space where k obstacles intersect is the *k-boundary face* and is defined as

$$
C_{i_1 \ldots i_k} = \{x \in \mathcal{F}_{i_1 \ldots i_k} \text{ such that } D(x) = 0\}. \tag{14}
$$

In m dimensions, an $(m-1)$-boundary face is termed a *boundary edge* and is illustrated in Figure 10. *Boundary fragments* are connected subsets of the boundary edges and are denoted c_{ij} ($c_{ij} \subset C_{ij}$). Finally, in $\mathbb{R}^m$, an m-boundary face, i.e. a *boundary point*, is where the GVG edge and boundary edge meet. Boundary points are also nodes in the GVG.

A *floating k-boundary face*, $FC_{i_1 \ldots i_k}$ is the set of points in a k-equidistant face where at least two gradient vectors become collinear, i.e.,

$$
\begin{aligned}
FC_{i_1 \ldots i_k} = \{x \in \mathcal{F}_{i_1 \ldots i_k} : \ \nabla d_{j_1}(x) = \nabla d_{j_2}(x) \\
\text{where } j_1, j_2 \in \{i_1, \ldots, i_k\}\}.
\end{aligned}
\tag{15}
$$

Analogous to boundary edges, *floating boundary edges* are floating $(m-1)$-boundary faces in $\mathbb{R}^m$, and *floating boundary fragments* are connected subsets of the boundary edges and are denoted by fc_{ij}, where $fc_{ij} \subset FC_{ij}$. Just like boundary edges, in most environments, there are not that many floating boundary edges (and thus floating boundary fragments) because these structures are associated with the boundary of the environment.[1] Finally, *floating boundary points* are floating m-boundary faces in $\mathbb{R}^m$. See the appendix for an example containing boundary and floating boundary edges.

The following proposition guarantees that the $(k+1)$-equidistant face, the k-boundary face, and the floating k-boundary face are the only structures that can exist in the boundary of a k-equidistant face.

PROPOSITION 1. If a $(k+1)$-equidistant face $\mathcal{F}_{i_1 \ldots i_{k+1}}$ is nonempty, then the k-equidistant face $\mathcal{F}_{i_1 \ldots i_k}$ must also be nonempty; however, the converse is not necessarily true. Furthermore,

$$
\partial\mathcal{F}_{i_1 \ldots i_k} = \mathcal{F}_{i_1 \ldots i_k i_{k+1}} \bigcup C_{i_l \ldots i_k} \bigcup FC_{i_1 \ldots i_k}.
$$

---

1. Note that floating boundary faces can be defined alternatively via a *floating k-boundary surface*, $FS_{i_1 \ldots i_k}$, which is the set of points on the boundary of a k-equidistant surjective surface where two gradient vectors become collinear, i.e., $FS_{i_1 \ldots i_k} = \{x \in \mathcal{SS}_{i_1 \ldots i_k} : \ \nabla d_{j_1}(x) = \nabla d_{j_2}(x)$, where $j_1, j_2 \in \{i_1, \ldots, i_k\}\}$. Then $FC_{i_1 \ldots i_k} = \{x \in FS_{i_1 \ldots i_k} : \ \forall h \notin \{i_1, \ldots, i_k\}, d_h(x) \geq d_{i_1}(x) = \cdots = d_{i_k}(x)\}$.

The proof of the above proposition is a simple application of Equation 12 to the definition of a k-equidistant face, which is defined as

$$
\begin{aligned}
\mathcal{F}_{i_1 \ldots i_k} = \mathrm{cl}\{x \in \mathcal{W} : 0 < d_{i_1}(x) = \cdots = d_{i_k}(x) \\
\leq d_h(x) \ \forall h \\
\text{and } \nabla d_p(x) \neq \nabla d_q(x) \ \forall p, q \in \{i_1, \ldots, i_k\}\}.
\end{aligned}
$$

However, this proof can intuitively be derived by inspection of $\mathcal{F}_{i_1 \ldots i_k}$'s definition. Starting from the left-hand side of the definition, the portion of the boundary associated with the first inequality, $0 < d_{i_1}(x) = \cdots = d_{i_k}(x)$, is the set of points where $0 = d_{i_1}(x) = \cdots = d_{i_k}(x)$; this is a k-boundary face, $C_{i_1 \ldots i_k}$. The portion of the boundary associated with the next inequality, $d_{i_1}(x) = \cdots = d_{i_k}(x) \leq d_h(x)$, is the set of points equidistant to $k+1$ obstacles, i.e., a $(k+1)$-equidistant face. Finally, the set of points on the boundary associated with the final inequality, $\nabla d_p(x) \neq \nabla d_q(x)$, is a floating k-boundary face, $FC_{i_1 \ldots i_k}$.

3.3. Generalized Voronoi Graph Definition

With the equidistant faces and other structures, we can now define the GVG as follows:

DEFINITION 3. The *generalized Voronoi graph* (GVG) is a graph embedded in $\mathbb{R}^m$ whose edges are m-equidistant faces and whose nodes are $m+1$ equidistant faces, m-boundary faces, and m-floating boundary faces, i.e.,

$$
\begin{aligned}
GVG = \Big[\Big(\bigcup \mathcal{F}_{i_1 \ldots i_m} \Big), \\
\Big(\bigcup \mathcal{F}_{i_1 \ldots i_{m+1}} \bigcup C_{i_1 \ldots i_m} \bigcup FC_{i_1 \ldots i_m} \Big) \Big].
\end{aligned}
\tag{16}
$$

In other words, GVG comprises edges, the GVG edges, and the nodes, which include meet points, boundary points, and floating boundary points. Please note the union operator ($\bigcup$) was loosely used in the above definition to mean the union over all possible indices.

EXAMPLE 1. Figure 11 depicts a generalized Voronoi graph for a rectangular enclosure in $\mathbb{R}^3$. The GVG edges, delineated by solid lines, constitute the locus points equidistant to three obstacles, and the meet points are where the GVG edges intersect. There are eight GVG edges that look like spokes; these have boundary points, in addition to meet points, as end points.

3.4. Dimension of GVG Components

The GVG is the backbone of the HGVG roadmap, and therefore we must first show that it is truly one-dimensional. To determine the generic dimension of the GVG edges, we will use the preimage theorem below to show that the GVG is

one-dimensional. To properly invoke the preimage theorem to obtain a correct dimension count, we first introduce an important transversality assumption and discuss its implications.

ASSUMPTION 2. Equidistant Surface Transversality Assumption: If equidistant surjective surfaces are manifolds, then they intersect transversally. That is, $SS_{i_1...i_k j_1} \bar{\pitchfork} SS_{i_1...i_k j_2}$ with respect to $SS_{i_1...i_k}$ if $j_1 \neq j_2$.

In the case that $m = 2$ and the obstacles are points, this assumption is equivalent to the "no four points are co-circular" assumption, which is often made in the Voronoi diagram literature (Aurenhammer 1991). Assumption 2 is the generalization of this statement.

This transversality assumption can also be interpreted as an assumption on the stability of the equidistant surface intersection geometry. In Figure 12, $SS_{ijk} = SS_{jkl} = SS_{ikl} = SS_{ijl}$ because there exists a circle that intersects the four obstacles (a nongeneric case). After a slight perturbation of the obstacles, the equidistant surfaces no longer coincide (Fig. 13). Since SS_{ijk} and SS_{ijl} are points in this example, they intersect transversally only if they do not intersect at all. As a result of Assumption 2, $SS_{i_1...i_k j_1} \neq SS_{i_1...i_k j_2}$ if and only if $j_1 \neq j_2$. The condition where two equidistant surjective surfaces are equal is an unstable nongeneric one, and thus we do not consider it because any slight perturbation of the obstacle locations drastically affects equidistance relationships. With this assumption in place, we are now ready to determine the generic dimension of the GVG.
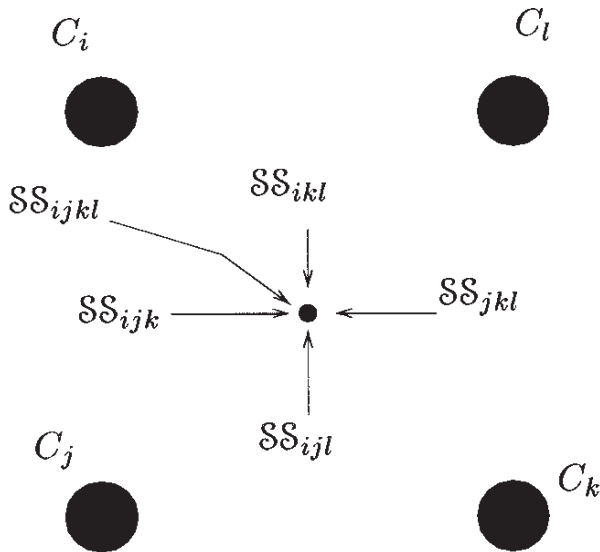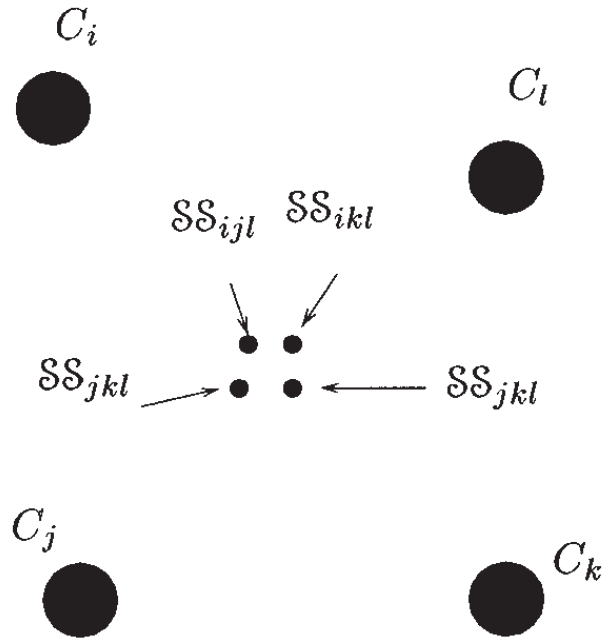

Fig. 12. Nongeneric arrangement.

Fig. 13. Small perturbation in obstacle locations.

Let the mapping $G : \mathbb{R}^m \rightarrow \mathbb{R}$ be defined as

$$G(x) = \begin{bmatrix} (d_{i_1} - d_{i_2})(x) \\ (d_{i_1} - d_{i_3})(x) \\ \vdots \\ (d_{i_1} - d_{i_m})(x) \end{bmatrix}.$$

An m-equidistant surjective surface can be defined as preimage of zero under that mapping G. That is, $SS_{i_1...i_m} = G^{-1}(0)$. Assumption 2 ensures that zero is always a regular value of G for all points x in the surjective surface $SS_{i_1...i_m}$. Therefore, the preimage theorem (also known as the submersion theorem) (Abraham, Marsden, and Ratiu 1988) asserts that $SS_{i_1...i_m}$ is one-dimensional.

By a similar argument, $m + 1$-equidistant surjective surfaces, m-boundary faces, and floating m-boundary surfaces are zero-dimensional.

Since the GVG edges are subsets of m-equidistant surjective surfaces, they could have a dimension as high as one, but not necessarily one. First, we need to establish that the interior of the GVG edges are one. We do this via the following lemma:

LEMMA 1.   The interior of the k-equidistant face, interior $(\mathcal{F}_{i_1...i_k})$, has the same dimension as the k-equidistant surjective surface, $SS_{i_1...i_k}$.

Proof. The interior of the k-equidistant face, interior$(\mathcal{F}_{i_1...i_k})$, has the property that for all $x \in \mathcal{FS}$, $d_{i_1}(x) = \cdots = d_{i_k}(x) < d_h(x)$ $\forall h \notin \{i_1, \ldots, i_k\}$. Let $x \in$ interior$(\mathcal{F}_{i_1...i_k})$. Therefore, $x \in SS_{i_1...i_k}$. At a point x where $d_{i_1}(x) = $

$\cdots = d_{i_k}(x) < d_h(x)$, there exists an nbhd$(x)$ in $SS_{i_1\ldots i_k}$. Let $Y = \text{nbhd}(x) \bigcap SS_{i_1\ldots i_k}$. To show that interior$(\mathcal{F}_{i_1\ldots i_k})$ has the same dimension as $SS_{i_1\ldots i_k}$, it suffices to show that $Y \subset \text{interior}(\mathcal{F}_{i_1\ldots i_k})$.

Since $x \in \text{interior}(\mathcal{F}_{i_1\ldots i_k})$, there exists an $h \notin \{i_1, \ldots, i_k\}$ such that $d_{i_1}(x) = \cdots = d_{i_k}(x) < d_h(x)$. By continuity of the single object distance function, for ϵ sufficiently small, $d_{i_1}(x + \epsilon) = \cdots = d_{i_k}(x + \epsilon) < d_h(x + \epsilon)$. Therefore, Y is an open subset of interior$(\mathcal{F}_{i_1\ldots i_k})$, and thus the dimensions of $SS_{i_1\ldots i_k}$ and interior$(\mathcal{F}_{i_1\ldots i_k})$ are the same. $\square$

Now, we can show the following:

PROPOSITION 2.   The GVG edges are one-dimensional with zero dimensional boundary.

Proof. Since $SS_{i_1\ldots i_{m+1}}$ is a zero-dimensional manifold, it consists of isolated points in $\mathcal{W} \backslash \bigcup_{h=1}^m C_h$. Each of these points is an open set in the topology that $\mathcal{W} \backslash \bigcup_{h=1}^m C_h$ induces on $SS_{i_1\ldots i_{m+1}}$. Furthermore, nonempty subsets of a collection of points are points, and thus all nonempty subsets of $SS_{i_1\ldots i_{m+1}}$ are open sets in the subspace topology. Since $\mathcal{F}_{i_1\ldots i_{m+1}}$ is a nonempty subset of $SS_{i_1\ldots i_{m+1}}$, $\mathcal{F}_{i_1\ldots i_{m+1}}$ is zero-dimensional. By a similar argument $C_{i_1\ldots i_m}$ and $FC_{i_1\ldots i_m}$ are zero-dimensional.

By Proposition 1, $\mathcal{F}_{i_1\ldots i_m}$ can be defined as

$$\text{interior}(\mathcal{F}_{i_1\ldots i_m}) \bigcup_\beta \mathcal{F}_{i_1\ldots i_m k_\beta} \bigcup C_{i_1\ldots i_m} \bigcup FC_{i_1\ldots i_m}.$$

Since $\forall \beta$, $\mathcal{F}_{i_1\ldots i_m k_\beta} \bigcup C_{i_1\ldots i_m} \bigcup FC_{i_1\ldots i_m}$ is zero-dimensional and interior$(\mathcal{F}_{i_1\ldots i_m})$ is one-dimensional, the GVG edge, $\mathcal{F}_{i_1\ldots i_m}$, is a one-dimensional manifold with a zero-dimensional boundary. $\square$

The procedure described in the above paragraph can be repeated to show that any k-equidistant face is $(m - k + 1)$-dimensional.

3.5. Accessibility

As stated in the previous section, the GVG is the backbone of the HGVG roadmap. Therefore, if the GVG has the accessibility property, so does the HGVG. In this section, we give an argument that a path exists from any point in the free space to a GVG edge, i.e., the GVG has the roadmap accessibility property.

PROPOSITION 3.   Given the Boundedness Assumption and the Equidistant Surface Transversality Assumption, the GVG has the property of accessibility.

Proof. We demonstrate that a robot can access the GVG by following a path that is constructed using gradient ascent on the multiobject distance function $D(x)$, which is the distance to the nearest object from x. Although $D(x)$ is not smooth, the multiobject distance function does possess a *generalized gradient*, which is denoted

$$\partial D(x) = \text{Co}\{\nabla d_i(x): \forall i \in I(x)\}. \qquad (17)$$

Furthermore, it is shown (Choset and Burdick 1994) that if $0 \in \text{interior}(\partial D(x))$, where 0 is the origin of the tangent space at x, then x is a local maxima of D. Using this result and the following two lemmas, we can conclude that if x is a local maxima of D, then the point x is equidistant to $m + 1$ obstacles.

LEMMA 2.   Given a set of n arbitrary vectors in $\mathbb{R}^m$, then $0 \in \text{interior}(\text{Co}\{v_i \in \mathbb{R}^m: i = 1, \ldots, n\})$ if and only if $\{v_i \in \mathbb{R}^m: i = 1, \ldots, n\}$ positively span $\mathbb{R}^m$.

LEMMA 3.   Goldman and Tucker. It requires a minimum of $(m + 1)$ vectors to positively span $\mathbb{R}^m$.

The results of Scheimberg and Oliveira (1992) can be extended to show that the generalized gradient of D only vanishes at a local minima. Assume the robot does not start at a local minima (this assumption is reasonable because we are performing a gradient ascent operation and the local minima are generically isolated unstable extrema points that occur on a set of measure zero). Therefore, gradient ascent of the multiobject distance function will bring the robot to a local maxima of D, which is a point equidistant to $m + 1$ obstacles, which is a point on the GVG. (Note that when ∂D is a set, the vector with the smallest norm in ∂D is chosen as the gradient (Scheimberg and Oliveira 1992). $\square$

The explicit numerical implementation of the gradient ascent operation is described in the companion paper (Choset and Burdick 2000).

3.6. Departability

Departability is the property of a roadmap that ensures all points are accessible from at least one point in the roadmap (Rimon and Canny 1994). In the case where full knowledge of the world's geometry is available, departability is simply accessibility, but in reverse. The "on-line" case is considered in the companion paper (Choset and Burdick 2000).

3.7. Connectivity of the GVG

When the GVG is connected, it is a roadmap in its own right, and thus sufficient for motion planning. The GVD is connected (Ó'Dúnlaing and Yap 1985; Choset 1996), and thus for planar environments ($m = 2$), the GVG is connected. Yap demonstrates a condition in Schwartz and Yap (1987) that ensures connectivity of the GVG in any dimension, as follows. The generalized Voronoi regions and equidistant faces may be viewed as a cellular decomposition of $\mathcal{W}$ into k-dimensional sets, where $k = 0, \ldots, m$. If each k-dimensional cell is homeomorphic to a k-dimensional disk, then the one-dimensional cells of such a decomposition form a roadmap

structure of $\mathcal{W}$ (Schwartz and Yap 1987). The GVG is sufficient for motion planning in any dimensioned configuration spaces if all equidistant faces satisfy this condition. For example, the equidistant faces in Figure 11 satisfy this condition and hence the GVG is connected.

4. The Hierarchical Generalized Voronoi Graph

The GVG is a great strategy for motion planning in all planar environments, and some multidimensional ones under certain conditions. In environments where these conditions are not upheld, the GVG is not sufficient for general purpose motion planning because the GVG is not connected. These environments are realistic and are not mathematical nongeneric cases. For example, Figure 14 contains an example of a disconnected GVG with two connected components: (1) an outer GVG network similar to the one described in Example 1 and (2) an inner GVG network that forms a halolike structure around the inner box. Solving this connectivity problem is a major contribution of this work.

The two-equidistant face defined by the floor and the ceiling in Figure 14 violates Yap's condition because the face is not homeomorphic to a two-dimensional disk, i.e., the halolike boundary structure forms a hole in the middle of the face. In this section, we define additional structures, termed *higher order generalized Voronoi graphs*, and use them to connect the disconnected boundaries of two-equidistant faces, which in turn connect the GVG. Essentially, higher order generalized Voronoi graphs are like GVGs that are recursively defined on lower dimensional equidistant faces. The HGVG is the GVG and all higher order generalized Voronoi graphs.

For the rest of this paper, we will focus attention on developing a roadmap for $\mathbb{R}^3$, even though many of the following results are general to $\mathbb{R}^m$. Since we are only considering $\mathcal{W} \subset \mathbb{R}^3$, then

- the only higher order generalized Voronoi graph is a second-order generalized Voronoi graph,

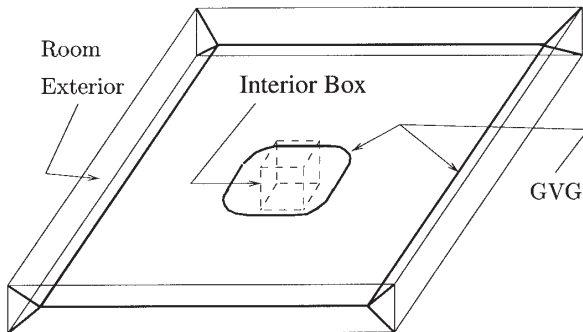- two-equidistant faces are two-dimensional, and

Fig. 14. An example of a disconnected GVG.

- GVG edges are three-equidistant faces formed by the intersection of *three* two-equidistant faces.

The underlying philosophy of the HGVG is to exploit the connectivity property of the GVD, the union of the two-equidistant faces. By definition, GVG edges lie on the boundaries of two-equidistant faces, and thus adjacent two-equidistant faces share a common GVG edge. If the GVG edges associated with each two-equidistant face were connected (i.e., the boundary of each two-equidistant face is connected according to Yap's assumption), then the entire GVG is connected because the GVD is connected.

When the GVG is disconnected, a two-equidistant face has a disconnected boundary. However, the HGVG connects disconnected boundary components on each two-equidistant face, and thus the HGVG is connected because the GVD is connected. Now, our goal is to use the second-order GVG, denoted with a superscript GVG^2, to connect the boundaries of two-equidistant faces with disconnected boundary components, thereby connecting all disconnected GVG components. In this section, we explicitly define the HGVG in $\mathbb{R}^3$ and supply a connectivity proof that makes an assumption. The ensuing sections relax this assumption, while maintaining connectivity of the HGVG. Finally, Assumption 1 has to be modified to make sure there are "enough" obstacles for the following.

4.1. GVG² Equidistant Edges

The construction of the GVG^2 parallels that of the GVG. The basic building block of the GVG^2 is called the *second-order two-equidistant surface* and is defined as $\mathcal{S}_{kl}|_{\mathcal{F}_{ij}} = \{x \in \mathcal{F}_{ij} : (d_l - d_k)(x) = 0\}$. Of particular interest is a subset of $\mathcal{S}_{kl}|_{\mathcal{F}_{ij}}$ termed the *two-equidistant surjective surface*, which is defined as $\mathcal{SS}_{kl}|_{\mathcal{F}_{ij}} = \text{cl}\{x \in \mathcal{S}_{kl}|_{\mathcal{F}_{ij}} : \nabla d_l(x) \neq \nabla d_k(x)\}$. We define the *second-order two-equidistant face* to be

$$\mathcal{F}_{kl}|_{\mathcal{F}_{ij}} = \{x \in \text{cl}(\mathcal{SS}_{kl}|_{\mathcal{F}_{ij}}) : \forall h, \, d_h(x) \geq d_k(x)$$

$$= d_l(x) \geq d_i(x) = d_j(x)\}. \tag{18}$$

The second-order two-equidistant face, $\mathcal{F}_{kl}|_{\mathcal{F}_{ij}}$, is the set of points on the face, $\mathcal{F}_{ij}$, that are equidistant to two obstacles C_k and C_l such that C_k and C_l are the *second* closest equidistant objects and C_i and C_j are the closest equidistant obstacles. In Figure 15, the lower-left dotted edge is the set of points whose *closest* equidistant obstacles are the floor and ceiling and whose second closest obstacles are the left and front walls.[2] This edge is a second-order two-equidistant edge.

---

2. Note that we are counting first and second closest differently than one would rank winners of a car race. In a race, if two cars tie for first, then the next car is considered to be "third." In our counting of first, second, etc., we would consider the next car to be "second." Also, we presume that Assumption 1 ensures there are enough obstacles to define the second-order equidistant faces.

Analogous to the GVG, we continue our construction with lower dimensional subsets of $\mathcal{F}_{ij}$. The *second-order three-equidistant face*,

$$\mathcal{F}_{klp}|_{\mathcal{F}_{ij}} = \mathcal{F}_{kl}|_{\mathcal{F}_{ij}} \bigcap \mathcal{F}_{lp}|_{\mathcal{F}_{ij}} \bigcap \mathcal{F}_{kp}|_{\mathcal{F}_{ij}},$$

is the set of points where C_k, C_l, and C_p are *second* closest equidistant objects and C_i and C_j are the closest equidistant objects.

Continuing in this vein, we can define second-order k-equidistant faces, but since we are limiting the discussion to $\mathbb{R}^3$, the second-order two-equidistant faces are the GVG^2 edges, and the second-order three-equidistant faces are the second-order meet points.[3]

The dotted lines in Figure 15 are GVG^2 edges. Note that there is a "cycle" in the second-order GVG, which implies the existence of the GVG cycle inside of it. With this information, the robot makes a link from the second-order cycle to the GVG, thereby connecting the roadmap in this example. This linking strategy is defined in a later section.

4.2. Second-Order Generalized Voronoi Region

Recall from Section 3.1 that the GVD forms a complex that separates the robot's work space into generalized Voronoi regions, each of which is the set of points closest to a particular obstacle. Likewise, the GVG^2 constrained to a two-equidistant face, denoted GVG$^2|_{\mathcal{F}_{ij}}$, separates the two-equidistant face $\mathcal{F}_{ij}$ into *second-order generalized Voronoi regions*, each of which has a particular *second closest obstacle* (but C_i and C_j are the closest obstacles). The second-order generalized Voronoi regions are formally defined as

$$\mathcal{F}_k|_{\mathcal{F}_{ij}} = \mathrm{cl}\{x \in \mathcal{F}_{ij} : \forall h \neq i, j, k,$$
$$0 < d_i(x) = d_j(x) < d_k(x) < d_h(x)$$
$$\text{and } \nabla d_i(x) \neq \nabla d_j(x)\}. \quad (19)$$

EXAMPLE 2.   Let GVG$^2|_{\mathcal{F}_{\text{floor/ceiling}}}$ be the second-order GVG for the two-equidistant face, $\mathcal{F}_{\text{floor/ceiling}}$, defined by the floor and ceiling of the rectangular enclosure in Figure 15. The solid lines in Figure 15 represent the GVG, and the dotted lines represent GVG$^2|_{\mathcal{F}_{\text{floor/ceiling}}}$. The GVG$^2|_{\mathcal{F}_{\text{floor/ceiling}}}$ divides $\mathcal{F}_{\text{floor/ceiling}}$ into five regions whose closest obstacles are the floor and ceiling; furthermore, each region has a unique second closest obstacle: the front face, the right face, the back face, the left face, and the interior box. These regions are the second-order generalized Voronoi regions.

Just as the boundaries of the generalized Voronoi regions define the GVD, the boundaries of the second-order general-

Fig. 15. Box in a room.

ized Voronoi regions constitute the second-order generalized Voronoi graph, i.e., GVG$^2|_{\mathcal{F}_{ij}} = \bigcup_k \partial \mathcal{F}_k|_{\mathcal{F}_{ij}}$.

If the boundaries of each second-order generalized Voronoi region are connected (or can be connected with a link), then the boundaries of the two-equidistant faces, i.e., the GVG edges, are connected through the second-order generalized Voronoi graph. Therefore, our goal now is to ensure the boundaries of the second-order generalized Voronoi regions are connected or can be connected via a well-defined link.

However, before we can discuss connecting the boundaries of the second-order generalized Voronoi regions, we must first identify all of the structures in their boundaries. Unlike the case in Figure 15, the second-order GVG may contain other structures. These additional structures are boundary edges, floating boundary edges, and *occluding edges*. Since there are many types of GVG^2 edges, the structures defined in Section 4.1 are termed *GVG^2 equidistant edges*. These edges are similar to GVG edges because they are defined in terms of equidistant relationships. The boundary edges defined in Section 3.2 have their name because they exist on the boundary of the environment; in $\mathbb{R}^3$, they are the set of points where the distance to two obstacles is zero. Floating boundary edges are similar to boundary edges, but "float" in space. The final edges—occluding edges—are defined in the next section.

4.3. Occluding Edges

The following example motivates the need for an occluding edge.

EXAMPLE 3.   Hole on top of a box: Figure 16 depicts a flat room with a box in the middle of the room. The box in the middle of the room contains an opening that can either be a through-hole, a dimple, or an entrance to another internal environment.

The GVG structure associated with the box and the hole (see Fig. 17) contains two connected components: one associated with the hole and ceiling, and one associated with

---

3. It is worth noting that to define the GVG^2 edges, Assumption 1 must be upgraded to ensure there are "enough" obstacles to form one-dimensional structures. Hence, the GVG and GVG^2 in higher dimensions require a cluttered environment with at least $m + 1$ obstacles, where m is the dimension of the space.
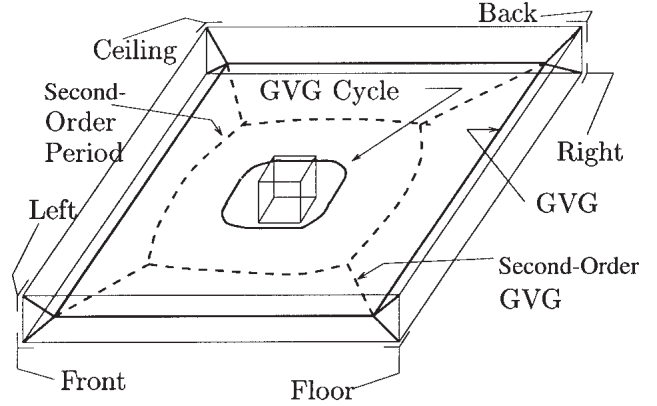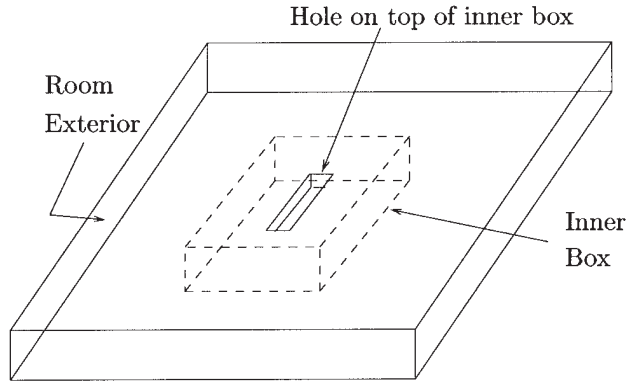
Fig. 16. Room with a box in the middle. The box, outlined with dotted lines, has an opening on top of it, delineated with solid lines.
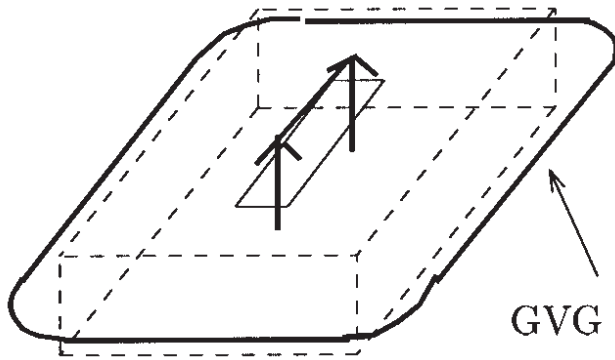

Fig. 17. The GVG edges in the vicinity of the interior box. This halo-shaped GVG edge is defined by the ceiling, floor, and box. The two parallel arrowlike structures connected by a segment is the GVG structure defined by the four sides of the hole and the ceiling.

the box, the floor, and the ceiling. Unfortunately, the two connected components are not within line of sight of each other. Hence, even if the robot possessed a magical "GVG sensor," depending on the robot's initial conditions, it may "miss" one of these connected components while incrementally constructing the HGVG. Therefore, there is a need to define an additional structure to link the disconnected connected components.

DEFINITION 4. The *two-occluding face*, $V_{kl}|_{\mathcal{F}_{ij}}$, is the set of points on the shared boundary of two adjacent second-order generalized Voronoi regions, $\mathcal{F}_k|_{\mathcal{F}_{ij}}$ and $\mathcal{F}_l|_{\mathcal{F}_{ij}}$, where for $x \in V_{kl}|_{\mathcal{F}_{ij}}$, $s \in \mathcal{F}_k|_{\mathcal{F}_{ij}}$, and $t \in \mathcal{F}_l|_{\mathcal{F}_{ij}}$, $\lim_{s \to x} d_k(s) \neq \lim_{t \to x} d_l(t)$.

The occluding faces make the bridge between disconnected GVG components that are not within line of sight of each other. In $\mathbb{R}^3$, a two-occluding face is called an *occluding edge*.

Connected subsets of an occluding edge are termed *occluding fragments* and are denoted v_{ij}. The following example gives an intuitive description of the occluding edges.

EXAMPLE 4. Occluding Edge: Recall the rectangular enclosure with a box in its interior in Figure 15. Consider the two-equidistant face defined by the box and the ceiling of Figure 15. This two-equidistant face is shaped like an upside-down bowl, as depicted in Figure 18. Figure 19 contains a side view of Figure 18.

Consider a robot in Figure 19 that moves from left to right while maintaining double equidistance between the inner box and ceiling (i.e., while it remains on a two-equidistant face). Assume the robot starts at a point where the second closest obstacle is the floor. While moving from left to right on the two-equidistant face, the inner box begins to occlude the floor as the robot begins to pass over the box. (Recall that we are using the visible distance function.) When the floor becomes occluded, there is a discontinuous jump in the value of the distance to the second closest obstacle. The point where the floor becomes occluded is a point in an occluding edge.

The dashed lines in Figure 18 represent the occluding edge in the two-equidistant face defined by floor and ceiling. The occluding edge encloses a region where points in its exterior are within line of sight of the floor. (See Fig. 20.)

4.4. Structures of the Second-Order Generalized Voronoi Graph (Boundary Elements of the Second-Order Generalized Voronoi Regions)

Since the boundaries of the second-order generalized Voronoi regions constitute the second-order generalized Voronoi graph, we now consider them carefully. The following propo-
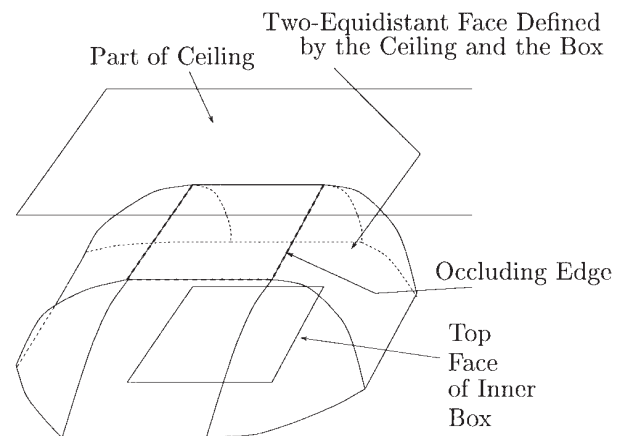

Fig. 18. Two-equidistant face between the box and the ceiling (from Fig. 14) is outlined with thin solid lines. All of the enclosure and box from Figure 14 is removed with the exception of the top of the box and the ceiling of the enclosure. Dashed lines delineate an occluding edge.
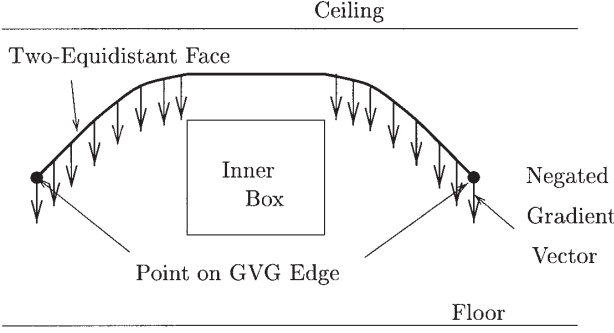
Fig. 19. The thick solid line represents a side view of the equidistant face defined by the box and the ceiling. The thick arrows that are distributed along the face point toward the floor, which is the second closest obstacle. There are no arrows on the portion of the face above the box because the box occludes the floor in that region.
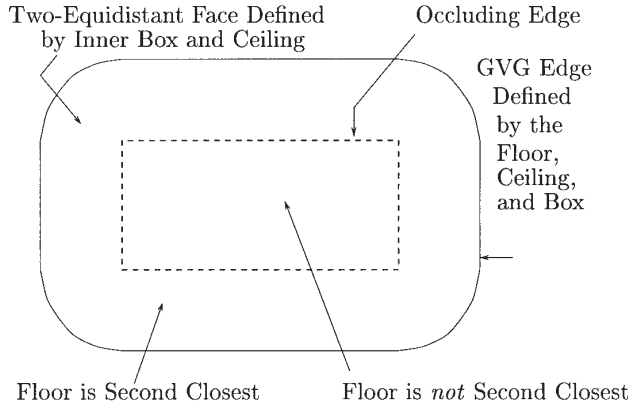

Fig. 20. Two-equidistant face between the box and the ceiling, as viewed from above, is drawn with an occluding edge.

sition enumerates the boundary structures of a second-order generalized Voronoi region:

PROPOSITION 4. In $\mathbb{R}^m$, the boundary of a second-order generalized Voronoi region may contain the following structures: two-equidistant faces, second-order two-equidistant faces, two-boundary faces, floating two-boundary faces, and two-occluding faces.

The proof of the above proposition in $\mathbb{R}^m$ is an application of eq. (12) through eq. (19); inspection of eq. (12) yields the boundary components of a second-order generalized Voronoi region in $\mathbb{R}^3$. Starting from the left, consider the first inequality, $0 < d_i(x) = d_j(x)$. The boundary associated with this inequality is the set of points where $0 = d_i(x) = d_j(x)$; this corresponds to a *boundary edge*. Consider the next inequality, $d_i(x) = d_j(x) < d_k(x)$, whose associated boundary is the set of points, $d_i(x) = d_j(x) = d_k(x)$; this corresponds to a *GVG edge*. The next inequality, $d_k(x) < d_h(x)$, is associated with a

common boundary of two adjacent second-order generalized Voronoi regions. When the distance to the second closest obstacle continuously changes as a robot crosses from one region to another (i.e., $d_i(x) = d_j(x) < d_k(x) = d_l(x) < d_h(x)$), the corresponding structure is a *GVG^2 equidistant edge*. When the distance to the second closest obstacle does *not* continuously change, the corresponding structure is an *occluding boundary edge*. The final boundary structure occurs when two gradients become collinear ($\nabla d_i(x) = \nabla d_j(x)$); this structure is a *floating boundary edge*.

4.5. Hierarchical Generalized Voronoi Graph Definition

The $GVG^2|_{\mathcal{F}_{ij}}$ edges include boundary edges, floating boundary edges, $GVG^2|_{\mathcal{F}_{ij}}$ equidistant edges, and occluding edges. The nodes are boundary points, floating boundary points, second-order meet points, and occluding meet points. The $GVG^2|_{\mathcal{F}_{ij}}$ is these collection of edges and nodes, i.e.,

$$
\begin{aligned}
& GVG^2|_{\mathcal{F}_{ij}} = \\
& \left[\left(C_{ij} \bigcup FC_{ij} \bigcup \left(\bigcup_k \bigcup_l \left(\mathcal{F}_{kl}|_{\mathcal{F}_{ij}} \bigcup V_{kl}|_{\mathcal{F}_{ij}} \right) \right) \right), \right. \\
& \left. \left(C_{ijk} \bigcup FC_{ijk} \bigcup \left(\bigcup_k \bigcup_l \bigcup_p \left(\mathcal{F}_{klp}|_{\mathcal{F}_{ij}} \bigcup V_{klp}|_{\mathcal{F}_{ij}} \right) \right) \right) \right].
\end{aligned}
$$
(20)

5. Roadmap Properties of the Hierarchical Generalized Voronoi Graph

So now that we have defined the HGVG, we need to show that it is a roadmap, a one-dimensional structure that has three properties: accessibility, departability, and connectivity. Since the GVG possesses the property of accessibility and is part of the HGVG, the HGVG also has the property of accessibility. Loosely speaking, departability is a consequence of the fact that each obstacle is within line of sight of at least one point on the HGVG. Assume the goal is a point obstacle and create a new HGVG, termed the *virtual HGVG*. There exists a set of points U in the virtual HGVG, whose points are within line of sight of the goal; it can be shown that at least one point in U is in the HGVG (in fact, "most of U" is in the original HGVG). Therefore, there exists a point in the HGVG that is within line of sight of the goal. See Figures 21 and 22.

The rest of this section demonstrates that the HGVG is connected.

The proof of connectivity of the HGVG relies on the fact that the boundaries of individual second-order generalized Voronoi regions are connected, or can be readily connected with a well-defined link. For the sake of explanation, assume this to be true.
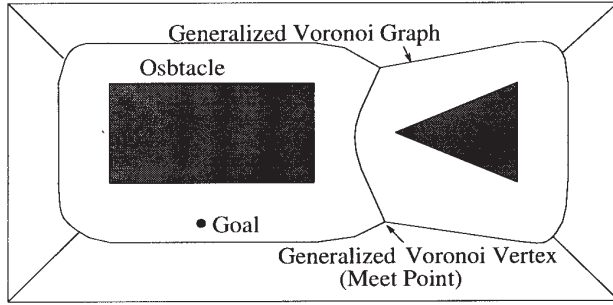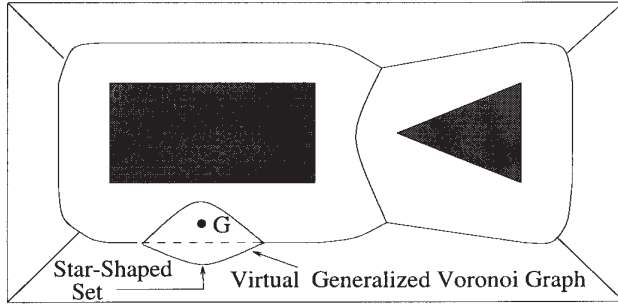
Fig. 21. The HGVG is a GVG in the plane.

Fig. 22. The virtual GVG.

PROPOSITION 5.   The HGVG (with its links) is connected.

Proof.   The proof of HGVG's connectivity is done in two steps: (1) show that the HGVG restricted to a two-equidistant face is connected, and then (2) demonstrate that all of the HGVGs restricted to all of the two-equidistant faces form a connected roadmap.

First by definition, the second-order generalized Voronoi regions, restricted to a two-equidistant face, form an exact cellular decomposition on that face. That is,

- $\bigcup_k \mathcal{F}_k|_{\mathcal{F}_{ij}} = \mathcal{F}_{ij}$,

- interior$(\mathcal{F}_k|_{\mathcal{F}_{ij}}) \bigcap$ interior$(\mathcal{F}_l|_{\mathcal{F}_{ij}}) = \emptyset$ $\forall k, l$,

- $\mathrm{cl}(\mathcal{F}_k|_{\mathcal{F}_{ij}}) \bigcap \mathrm{cl}(\mathcal{F}_l|_{\mathcal{F}_{ij}}) \neq \emptyset \iff \partial\mathcal{F}_k|_{\mathcal{F}_{ij}} \bigcap \partial\mathcal{F}_l|_{\mathcal{F}_{ij}} \neq \emptyset$.

Let q_s' and q_g' be two points on the boundary of second-order generalized Voronoi regions. Consider an arbitrary path $c : [0, 1] \to \mathcal{F}_{ij}$, where $c(0) = q_s'$ and $c(1) = q_g'$.

Now, we want to identify segments of this path with particular second-order generalized Voronoi regions. Let k be the index of the second-order generalized Voronoi region $\mathcal{F}_k|_{\mathcal{F}_{ij}}$. Let the mapping $f_c : \mathcal{F}_{ij} \to \{1, \ldots, n\}$ determine in which second-order generalized Voronoi region a point may lie, i.e., the index of the second-order generalized Voronoi region. This function will be piecewise constant.

The entire path is broken down into segments where each segment is a connected component of the preimage of a second-order generalized Voronoi region index under f_c. The end points of each segment lie on the boundary of its associated second-order generalized Voronoi region.

By construction, the concatenation of segments forms a path from start to goal. For each segment, there exists a connected path along the boundary of its associated region between the end points of the segment. Therefore, a new path can be constructed from the concatenations of these new boundary-connected path segments that connects q_s' and q_g' while remaining entirely on the boundaries of the second-order generalized Voronoi regions (see Figs. 23 and 24).

Since the selection of q_s' and q_g' was arbitrary, the union of the boundaries of the second-order generalized Voronoi regions is connected. That is, $\mathrm{GVG}^2|_{\mathcal{F}_{ij}}$ is connected. The second part of this proof uses this to show that the HGVG is connected in $\mathbb{R}^3$.

The GVD is connected (Ó'Dúnlaing and Yap 1985; Choset 1996); that is, the union of the two-equidistant faces is connected. Also, by definition adjacent two-equidistant faces share a common GVG edge. Therefore, the HGVG restricted to adjacent faces is connected. Since the union of the two-equidistant faces is connected, all of the HGVGs restricted to two-equidistant faces form a connected network. That is, the HGVG is connected. $\square$

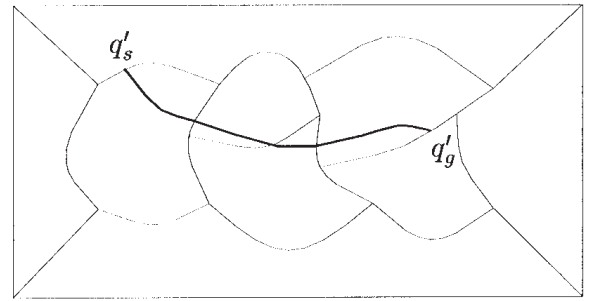**EXAMPLE 5.**   A connected HGVG: Figure 25 depicts the
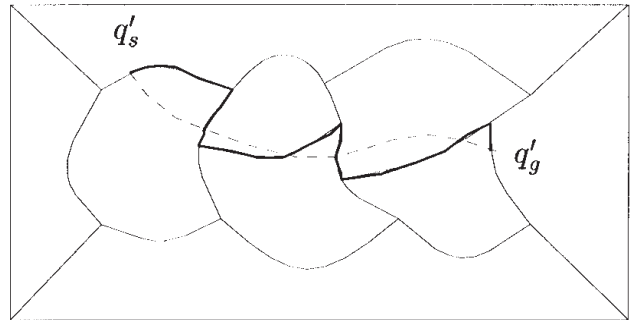

Fig. 23. Path in two-equidistant face.
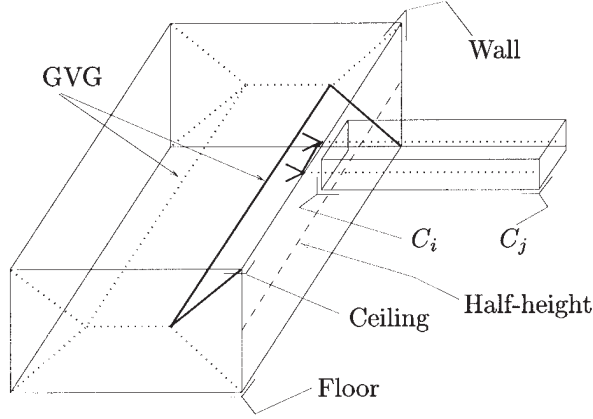

Fig. 24. Deformed path.

Fig. 25. A room with a hole in its side wall. The thick dotted lines represent the GVG and the thin dotted line marks the half-height of the room. The thick solid lines are drawn to emphasize the GVG edges associated with the two-equidistant face defined by the right wall and ceiling.

disconnected GVG for the environment shown in Figure 47, from Example 10.

The geometry of the hole with respect to the room causes the boundary of the two-equidistant face, defined by the wall and the ceiling in Figure 25, to be disconnected (Fig. 26); this results in a disconnected GVG. The second-order GVG prescribes a well-defined path on the two-equidistant face that connects the disconnected GVG fragments. Therefore, in this example the HGVG is connected (see Fig. 27).

Now, the HGVG connectivity proof hinges on the connectivity of the boundaries of the second-order generalized Voronoi regions, so the rest of this paper is devoted to this topic.

6. Cycles and Periods

When environments such as the one in Figure 15 have characteristics that give rise to cycles in the HGVG, the HGVG by itself is not necessarily connected. This section presents a strategy to resolve this issue. After defining the GVG cycle, we show that cycles cause the HGVG to be disconnected, because they give rise to second-order generalized Voronoi regions whose boundaries are not connected. Next, we demonstrate a duality between cycles in the second-order GVG and those in the GVG, which can give rise to a linking procedure to connect them. We also introduce an assumption that precludes the existence of cycles; this assumption is true in highly cluttered environments.

6.1. GVG Cycle

DEFINITION 5.   GVG Cycle: A *GVG cycle* is a GVG edge that is C^2-diffeomorphic to S^1, the unit circle.

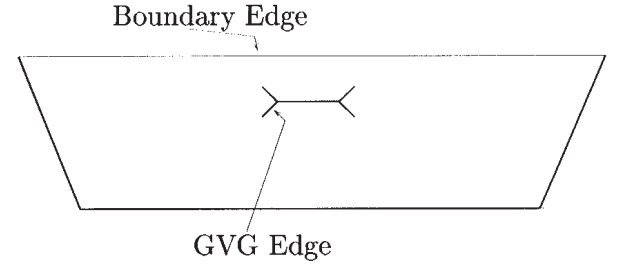Henceforth, the term "cycle" refers to a GVG cycle. In

Fig. 26. GVG edges, drawn as thick solid lines, are on the boundary of the two-equidistant face between the wall and the ceiling of Figure 25 in Example 10. The GVG structure in the middle of the face is associated with the hole; in actuality, it "pinches up" out of the face.
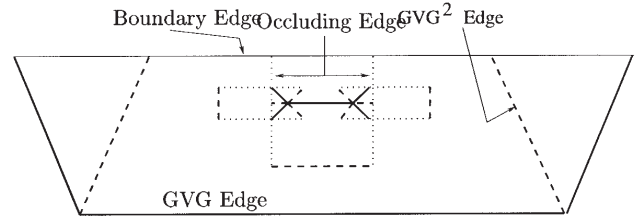

Fig. 27. The second-order GVG edges, boundary edges, and occluding edges are drawn in the two-equidistant face between the wall and the ceiling of Figure 25 in Example 10. The thick solid lines are GVG edges, the dotted lines are GVG^2 edges, the thin solid line is a boundary edge, and the thick dashed lines are the occluding edges. Here, the GVG^2 links up disconnected GVG edge fragments on the two-equidistant face.

Figure 14, the GVG cycle is the locus of points equidistant to the floor, ceiling, and interior box, which is the halolike structure that surrounds the box.

PROPOSITION 6.   In a bounded subset of a three-dimensional Euclidean space, a GVG edge is a cycle if and only if it is disconnected from all other edges in the GVG and the GVG^2.

Proof. This proof is a consequence of the following lemmas whose proofs appear in the appendix (Section B).

LEMMA 4.   When equidistant faces intersect transversally (Assumption 2 is upheld), a GVG cycle cannot contain a meet point.

LEMMA 5.   A GVG cycle cannot contain any boundary or floating boundary points.

LEMMA 6.   In $\mathbb{R}^3$, a three-equidistant surface, SS_{ijk}, is either C^2-diffeomorphic to S^1 (i.e., it is a GVG cycle) or it is unbounded.

LEMMA 7.   A GVG^2 equidistant edge can only intersect the GVG at a meet point.

If a GVG edge is a cycle, then it does not contain meet points (Lemma 4), boundary points (Lemma 5), or floating boundary points (Lemma 5), and thus it cannot intersect other GVG edges and GVG^2 edges (Lemma 7). That is, the GVG cycle is disconnected.

Assume there exists a disconnected GVG edge that is not a cycle. By Lemma 6, the GVG edge must be unbounded. However, this contradicts our Boundedness Assumption (Assumption 1), and thus the GVG edge is a cycle. $\square$

Whereas Proposition 6 states that the existence of GVG cycle implies that the HGVG is not connected, the next proposition demonstrates how cycles give rise to second-order generalized Voronoi regions whose boundaries are not connected.

PROPOSITION 7.   In a bounded subset of a three-dimensional Euclidean space, a GVG edge is a disconnected component of a boundary of a second-order generalized Voronoi region if and only if it is a cycle.

Proof. This proof is based on the following lemmas, whose results are general in $\mathbb{R}^m$ and whose proofs appear in the appendix.

LEMMA 8.   If the three-equidistant face $\mathcal{F}_{ijk}$ is not empty, then the second-order generalized Voronoi region $\mathcal{F}_k|_{\mathcal{F}_{ij}}$ must not be empty. Furthermore, if $\mathcal{F}_{ijk} \neq \emptyset$, then $\mathcal{F}_{ijk} \subset \mathcal{F}_k|_{\mathcal{F}_{ij}}$.

LEMMA 9.   The boundary of a second-order generalized Voronoi region contains at most *one* three-equidistant face. That is, $\mathcal{F}_{pqr} \subsetneq \mathcal{F}_k|_{\mathcal{F}_{ij}}$ for all $\{p, q, r\} \neq \{i, j, k\}$.

By Lemma 8, the GVG edge $\mathcal{F}_{ijk}$ must be a subset of the boundary of a second-order generalized Voronoi region, $\mathcal{F}_k|_{\mathcal{F}_{ij}}$. In fact, by Lemma 9 it is the only GVG edge that can be in the boundary of $\mathcal{F}_k|_{\mathcal{F}_{ij}}$. GVG^2 equidistant edges, boundary edges, floating boundary edges, and occluding edges (Proposition 4) are the other structures that *may* exist on the boundary of a second-order generalized Voronoi region.

If $\mathcal{F}_{ijk}$ is a cycle, then by Proposition 6 none of the above listed structures can intersect it, and thus $\mathcal{F}_{ijk}$ must lie on a disconnected component of the boundary of the second-order generalized Voronoi region.

If $\mathcal{F}_{ijk}$ is a disconnected boundary component of a second-order generalized Voronoi region, it does not intersect any GVG edge, or any GVG^2 edge. By Proposition 6, $\mathcal{F}_{ijk}$ is a cycle. $\square$

Recall Example 2, which consists of a room with a box in its interior. Figure 15 shows the two-equidistant face defined by the floor and ceiling. Solid lines represent the GVG, and dotted lines represent the GVG^2. The inner box defines a second-order generalized Voronoi region, $\mathcal{F}_{\text{box}}|_{\mathcal{F}_{\text{floor/ceiling}}}$. This region contains a cycle on its boundary and thus has a boundary that is not connected. All of the other second-order

generalized Voronoi regions do not contain any cycles and thus their boundaries are connected.

6.2. Second-Order Cycles and Periods

Just as there are cycles in the GVG, there are also cycles in the GVG^2. A *second-order cycle* is a GVG^2 equidistant edge that is C^2-diffeomorphic to S^1, the unit circle. However, we are interested in another structure, termed the *second-order period*, defined below.

DEFINITION 6.   GVG^2 Period: A *GVG^2 period* is a connected second-order generalized Voronoi region boundary component that does not contain any GVG edges.

By definition, a GVG^2 period is the union of zero or more GVG^2 equidistant edges, zero or more boundary fragments, zero or more floating boundary fragments, and zero or more occluding fragments. Note that second-order periods are homeomorphic to S^1 and that GVG^2 cycles are GVG^2 periods.

A GVG^2 period that only has GVG^2 equidistant edges is denoted $\bigcup_l \mathcal{F}_{kl}|_{\mathcal{F}_{ij}}$. A GVG^2 period that has GVG^2 equidistant edges, boundary fragments, floating boundary fragments, and occluding fragments is denoted by

$$C_{ij} \bigcup FC_{ij} \bigcup_l \left(\mathcal{F}_{kl}|_{\mathcal{F}_{ij}} \bigcup V_{kl}|_{\mathcal{F}_{ij}} \right).$$

For example, if a GVG^2 period is composed of three GVG^2 equidistant edges and one boundary edge, the GVG^2 period is $\mathcal{F}_{kl_1}|_{\mathcal{F}_{ij}} \bigcup \mathcal{F}_{kl_2}|_{\mathcal{F}_{ij}} \bigcup \mathcal{F}_{kl_3}|_{\mathcal{F}_{ij}} \bigcup C_{ij}$.

The second-order generalized Voronoi region, depicted in Figure 28, lies on the two-equidistant face defined by the floor and ceiling in Figure 15. This second-order generalized Voronoi region has as its closest obstacles the floor and ceiling and has as its second closest obstacle the inner box. The dotted lines on the outer boundary represent GVG^2 equidistant edges, which compose a GVG^2 period.

6.3. Inner and Outer Cycles and Periods

Here, we describe the notions of an inner and outer cycle. Recall the corollary to the Jordan curve lemma, which states that any closed curve in the plane (or surface diffeomorphic to a plane) divides the plane into two regions: one termed the *bounded* section and one termed the *unbounded* section.

Let $\partial_i \mathcal{F}_k|_{\mathcal{F}_{ij}}$ be a boundary component of the second-order generalized Voronoi region, $\mathcal{F}_k|_{\mathcal{F}_{ij}}$, and let it serve as a Jordan curve on $\mathcal{SS}_{ij}$. If $\mathcal{F}_k|_{\mathcal{F}_{ij}}$ lies on the bounded region of $\mathcal{SS}_{ij}$, then it is an *outer* boundary component. Otherwise, it is an *inner* boundary component. From these two definitions, the notion of an *inner cycle*, *outer cycle*, *inner GVG^2 period*, and *outer GVG^2 period* naturally follow.

EXAMPLE 6.   Figure 28 contains the second-order generalized Voronoi region that is defined by the box on the two-
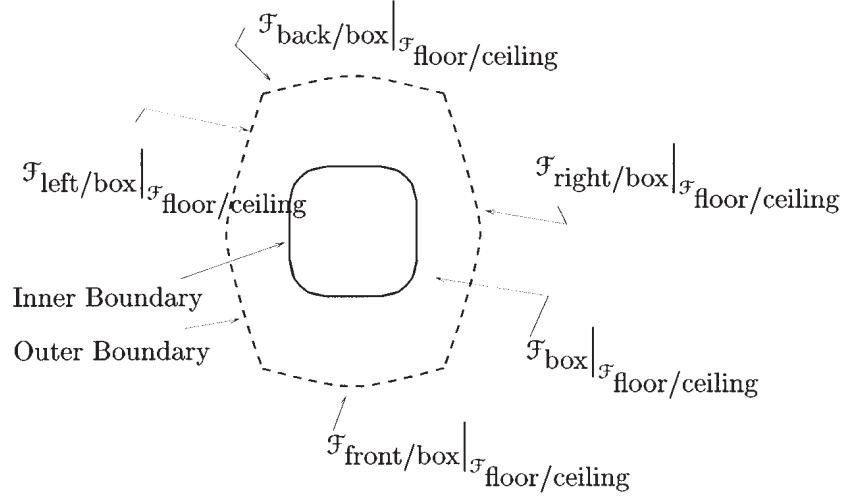
Fig. 28. The second order period is drawn with dotted lines. It is the union of second order GVG edges that forms a connected boundary component of a second order generalized Voronoi region.

equidistant face, defined by the floor and ceiling from Example 2. The dotted lines in Figure 28 represent the GVG^2 period that furnishes the outer boundary. The solid line represents the GVG cycle, which is an inner boundary component of $\mathcal{F}_{\text{box}}|_{\mathcal{F}_{\text{floor/ceiling}}}$. Figures 29 and 30 illustrate, respectively, how the definitions of inner and outer boundaries work. In Figure 29, when the GVG cycle is a Jordan curve, its associated second-order generalized Voronoi region lies in the unbounded region (shaded). Similarly, in Figure 30, when the GVG^2 period is a Jordan curve, its associated second-order generalized Voronoi region lies in the bounded region (shaded).

From Figures 15 and 28, it appears that there exists a duality between the existence of the GVG cycles and GVG^2 periods. The following proposition establishes this duality: for one of them to exist, the other must exist. Hence, the existence of one is a clue to the robot that another cycle or period is nearby. This information is needed for a "linking" strategy to connect disconnected HGVG components, such as those in Figure 15.

PROPOSITION 8. In $\mathbb{R}^3$, if a GVG cycle $\mathcal{F}_{ijk}$ is an inner boundary in a two-equidistant face $\mathcal{F}_{ij}$, then there exists an outer GVG^2 period in the two-equidistant face, $\mathcal{F}_{ij}$.

Proof. By Lemma 8, if $\mathcal{F}_{ijk} \neq \emptyset$, then the second-order generalized Voronoi region, $\mathcal{F}_k|_{\mathcal{F}_{ij}} \neq \emptyset$. Furthermore, Lemma 8 asserts that $\mathcal{F}_{ijk}$ is in the boundary of $\mathcal{F}_k|_{\mathcal{F}_{ij}}$. By Lemma 9, $\mathcal{F}_{ijk}$ is the only GVG edge in $\mathcal{F}_k|_{\mathcal{F}_{ij}}$. By the Boundedness Assumption (Assumption 1), $\mathcal{F}_k|_{\mathcal{F}_{ij}}$ must be bounded and thus contains an outer boundary component. According to Proposition 7, this outer boundary component does not contain $\mathcal{F}_{ijk}$. Such a boundary component is a GVG^2 period because it is free of GVG edges. □

Although the converse of the above statement is not nec-

essarily true, the following proves to be useful.

PROPOSITION 9. If the outer boundary of a second-order generalized Voronoi region is a GVG^2 period, and there is GVG edge associated with the same region, then the GVG edge is an inner GVG cycle.

Proof. Recall that a GVG^2 period cannot intersect with a GVG edge. By hypothesis, the GVG^2 period is an outer boundary. Also, by hypothesis, there exists a GVG edge, $\mathcal{F}_{ijk}$, inside the second-order period.

Assume that the edge $\mathcal{F}_{ijk}$ is not a cycle. If $\mathcal{F}_{ijk} \neq \emptyset$, then $\mathcal{SS}_{ijk} \neq \emptyset$ and by Lemma 6 it is unbounded. Therefore, $\mathcal{SS}_{ijk}$ must intersect the outer GVG^2 period. In particular, say $\mathcal{SS}_{ijk}$ intersects $\mathcal{F}_{kl}|_{\mathcal{F}_{ij}}$. For all $x \in \mathcal{SS}_{ijk} \bigcap \mathcal{F}_{kl}|_{\mathcal{F}_{ij}}$, $d_h(x) \geq d_i(x) = d_j(x) = d_k(x) = d_l(x)$, for all h. This is the definition of a meet point, and thus by Proposition 1, a GVG edge intersects $\mathcal{F}_{kl}|_{\mathcal{F}_{ij}}$. This contradicts our original hypothesis that $\mathcal{F}_{ijk}$ is a GVG^2 period. Therefore, $\mathcal{F}_{ijk}$ is a cycle. □

Linking from an outer second-order period to an inner GVG cycle is achieved via gradient descent of the distance to the second closest obstacle, constrained to a two-equidistant face. Let x be a point on a second-order period. Let C_i and C_j be the two closest obstacles, let C_k and C_l be the second closest obstacle, and let $\mathcal{F}_{ijk}$ be the inner GVG cycle. At x, $d_k(x) > d_i(x) = d_j(x)$.

Let $\pi_{T_x \mathcal{F}_{ij}} \nabla d_k(x)$ be the projection of the gradient $\nabla d_k(x)$ onto $T_x \mathcal{F}_{ij}$. This is the direction that increases distance to C_k while maintaining double equidistance between C_i and C_j. Continuity of the distance function guarantees that a path traced out by $\dot{c}(t) = -\pi_{T_{c(t)} \mathcal{F}_{ij}} \nabla d_k(c(t))$, where $c(0) = x$ encounters the inner GVG cycle if and only if $\nabla d_k(c(t))$ does not vanish. That is, the distance to C_k decreases as the distance
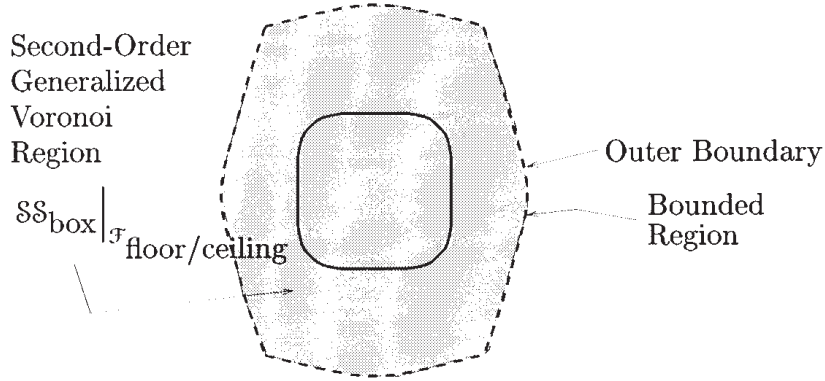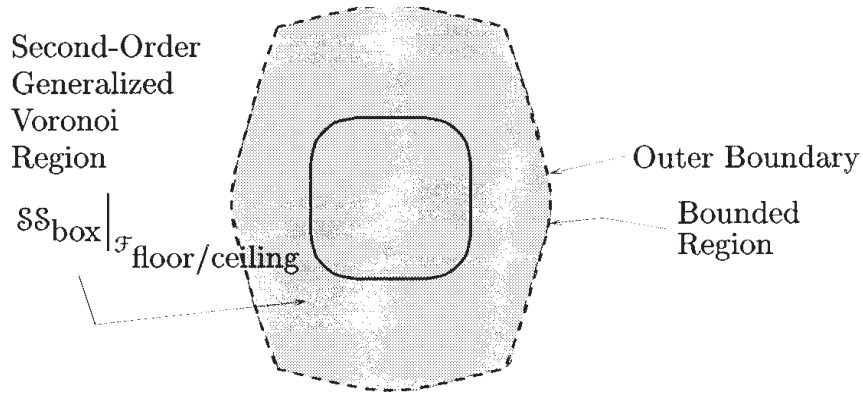
Fig. 29. Inner boundary.

Fig. 30. Outer boundary.

to C_i and C_j increases, or the distance to C_k decreases at a rate faster than the distance to C_i and C_j decrease. In either case, a link is made from the outer second-order period to an inner GVG cycle. See Figure 31 to see the linking procedure for the example originally found in Figure 14.

Finally, we must consider the situation when the gradient to the second closest obstacle constrained to a two-equidistant face vanishes. If the robot is performing gradient descent constrained to a two-equidistant face (i.e., $-\nabla d_k|_{\mathcal{F}_{ij}}$) from a GVG^2 equidistant edge $\mathcal{F}_{kl}|_{\mathcal{F}_{ij}}$ and the gradient vanishes, then there is no GVG edge (i.e., $\mathcal{F}_{ijk} = \emptyset$). In such a case, the robot simply returns to the outer boundary period.

Although the above linking procedure has been demonstrated in simulation, we are currently deriving a rigorous proof for it. However, we can introduce a well-stated assumption, which precludes the existence of cycles, thereby bypassing the need for the above linking procedure. This assumption is described in the following section.

6.4. Extended Boundedness Assumption

Now, we introduce an assumption that restricts the relative placement of obstacles in an environment such that no GVG
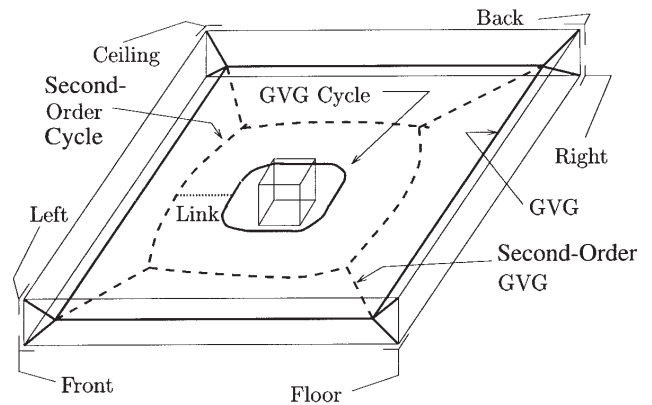

Fig. 31. Linking to and from cycles.

cycles can result. Also, when this assumption is upheld, all second-order generalized Voronoi regions contain one and only one GVG edge, which is useful for ensuring connectivity of the boundaries of second-order generalized Voronoi regions.

ASSUMPTION 3.   Extended Boundedness: In $\mathbb{R}^m$, each p-

order k-equidistant face has at least one p-order $(k + 1)$-equidistant face on its boundary.

In $\mathbb{R}^3$ ($m = 3$), this assumption implies that all GVG edges ($k = 3$, $p = 1$) contain at least one meet point. That is, for all i, j, k, there exists $x \in \mathcal{F}_{ijk}$ and there exists an l, such that $d_l(x) = d_k(x)$. By the Equidistant Surface Transversality Assumption (Assumption 2), this point is isolated.

Assumption 3 is not satisfied in the environment in Figure 15, which consists of a room with a box in its interior. There is a GVG edge that contains no meet points. However, when an additional box is placed into this environment, the HGVG *becomes connected* (see Fig. 32). The environment in Figure 32 satisfies the assumption because all GVG edges have meet points.

Now, we will show that when the Extended Boundedness Assumption is upheld in $\mathbb{R}^3$, all second-order generalized Voronoi regions posses a GVG edge, as shown by the following lemma. This result is used in demonstrating that environments that do not uphold the Extended Boundedness Assumption cannot have cycles.

LEMMA 10.   Let the Extended Boundedness Assumption (Assumption 3) and the visible distance function be in effect. In this case, all second-order generalized Voronoi regions must contain a three-equidistant face.

Proof. Recall the definition of the second-order generalized Voronoi region,

$$\mathcal{F}_k|_{\mathcal{F}_{ij}} = \{x \in \mathcal{F}_{ij} : \forall h \notin \{i, j, k\}\, d_h(x) \geq d_k(x) = d_i(x)\}.$$

Given the Extended Boundedness Assumption (Assumption 3), there exists an $h' \notin \{i, j\}$ and an x such that $d_i(x) = d_j(x) = d_{h'}(x)$. If $h' = k$, then $\mathcal{F}_{ijk} \neq \emptyset$, and by Lemma 8 and Lemma 9, it is the only three-equidistant face in $\partial \mathcal{F}_k|_{\mathcal{F}_{ij}}$.

If $h' \neq k$, then that implies $\mathcal{F}_{ijh'}$ must exist (i.e., there exists an x such that $d_i(x) = d_j(x) = d_{h'}(x)$). However,
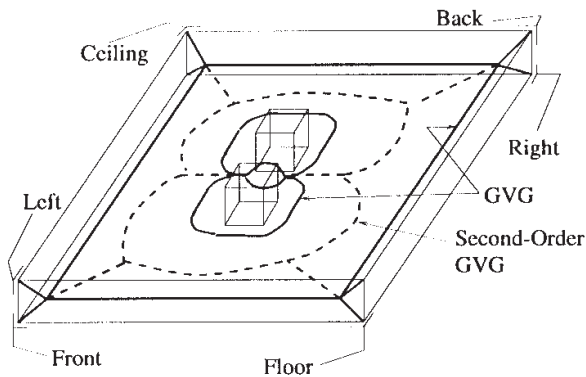

Fig. 32. Room with two boxes in its interior. The solid lines are GVG edges, and the dotted lines are GVG^2 edges.

since the second-order generalized Voronoi region $\mathcal{F}_k|_{\mathcal{F}_{ij}} \neq \emptyset$, it must be true that $d_k(y) \leq d_{h'}(y)$ for all $y \in \mathcal{F}_k|_{\mathcal{F}_{ij}}$. By continuity of the single object distance function, $\mathcal{F}_{ijk}$ must also be a nonempty subset of $\mathcal{F}_k|_{\mathcal{F}_{ij}}$ (Lemma 8). This is a contradiction of Lemma 9, where only one three-equidistant face may be a subset of $\mathcal{F}_k|_{\mathcal{F}_{ij}}$. Therefore, $h' = k$, and $\mathcal{F}_{ijk}$ is always a subset of $\mathcal{F}_k|_{\mathcal{F}_{ij}}$. □

LEMMA 11.   If Assumptions 2 and 3 hold, then there will be no GVG cycles, no GVG^2 cycles, and no outer GVG^2 periods.

Proof. Let $\mathcal{F}_{ijk}$ be a GVG edge in $\mathbb{R}^3$. By the Extended Boundedness Assumption (Assumption 3), there exists a point $x \in \mathcal{F}_{ijk}$ such that there is an obstacle C_l that is positioned such that $d_l(x) = d_k(x)$. Therefore, $\mathcal{F}_{ijkl} = \mathcal{F}_{ijl} \bigcap \mathcal{F}_{ijk} \neq \emptyset$. Since $\mathcal{F}_{ijk}$ is not disconnected from all other GVG edges, when the Equidistant Surface Transversality Assumption (Assumption 2) is in effect, Proposition 6 asserts that $\mathcal{F}_{ijk}$ is not a cycle.

By Proposition 9, if there exist (1) an outer second-order period, which is a component of the boundary of $\mathcal{F}_k|_{\mathcal{F}_{ij}}$, and (2) a generalized Voronoi edge, which is a subset of $\mathcal{F}_k|_{\mathcal{F}_{ij}}$ (whose existence is guaranteed by Lemma 11), then there exists a first-order cycle. The contrapositive of this statement is also true. If a GVG cycle does not exist, then an outer GVG^2 period cannot exist *or* the Extended Boundedness Assumption is not valid.

The Extended Boundedness Assumption implies that a GVG cycle cannot exist. This implies that an outer GVG^2 period cannot exist *or* the Extended Boundedness Assumption is not in effect. However, since the Extended Boundedness Assumption is in effect, there cannot be any outer GVG^2 periods. □

Note that this assumption requires use of the visible distance function. That is, the robot is only aware of obstacles that are within line of sight of it. Recall that all structures are defined in terms of the visible distance function. Also note that when this assumption is upheld, all second-order generalized Voronoi edges ($k = 2$, $p = 2$) have at least one second-order meet point.

Also note that the Extended Boundedness Assumption is a weak one. In $\mathbb{R}^m$ when $m > 2$, the Extended Boundedness Assumption is true for most "cluttered" work spaces. Robots whose configuration spaces are high dimensional tend to be highly articulated and are thus better suited for cluttered environments. Such environments do not contain cycles and thus may contain a connected HGVG.

6.5. Inner-Boundary Periods

Even when the Extended Boundedness Assumption is upheld, there are environments that contain an arrangement of obstacles that give rise to a disconnected HGVG. These periods are always inner periods on at least one two-equidistant sheet. This subsection introduces one of these periods termed

inner-boundary periods and describes a linking procedure that connects them.

EXAMPLE 7.   Inner Period: Figure 33 contains a room with four boxes floating in its interior. Two of the boxes, objects B_1 and B_2, are above box A_1. Boxes B_1 and B_2 have the same depth as box A_1.

Figure 34 depicts a cross-section of a three-dimensional world depicted in Figure 33. The cross-sections of the two-equidistant faces are drawn as solid lines and arc segments. The cross-sections of the GVG edges are points where three edges intersect and have circles drawn around them. Figures 35 and 36 display a top view of Figure 33. In these figures, the solid lines are the GVG edges and the dotted lines are the GVG^2 edges. In Figure 36, it can be seen that the second-order generalized Voronoi region has an outer and inner boundary. Lemma 12 allows for a link to be made between the two boundaries.

LEMMA 12.   Inner Boundary Link: If an inner GVG^2 period with GVG^2 edges exists on the boundary of the second-order generalized Voronoi region, then a link exists from the outer boundary to it.

Proof. By the Extended Boundedness Assumption (Assumption 3), if an inner GVG^2 period contains a GVG^2 edge, then
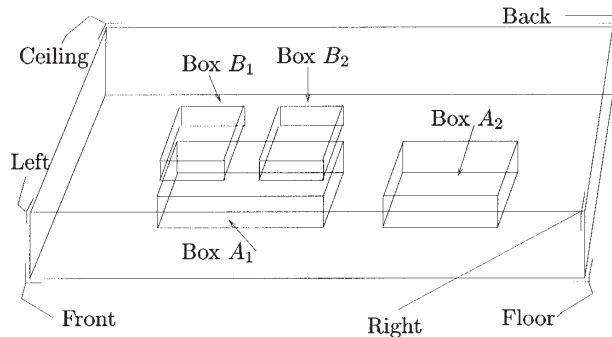

Fig. 33. A room with four boxes floating in its interior. Boxes B_1 and B_2 are floating above box A_1 and have the same depth as box A_1.
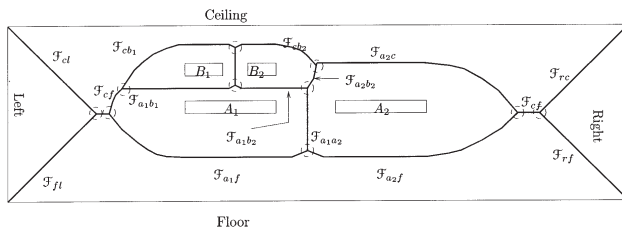

Fig. 34. Cross-section of the environment in Figure 33. The cross-section is parallel to the front face of the rectangular enclosure and cuts it through the three floating boxes. The solid lines are the two-equidistant faces, which meet at generalized Voronoi edges, which are circled.
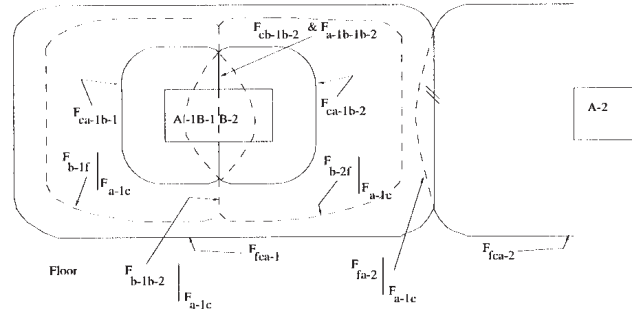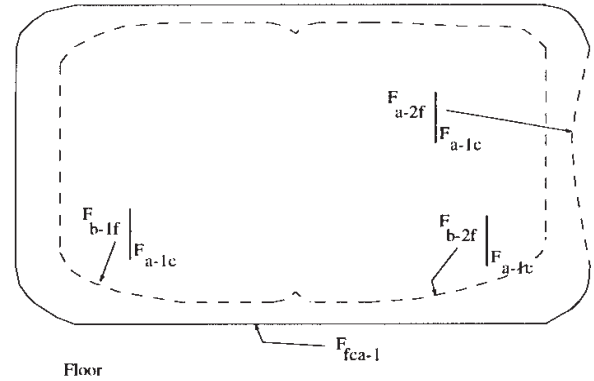

Fig. 35. GVG and GVG^2 edges (Top View).

Fig. 36. Inner Period.

it must contain a second-order meet point, $\mathcal{F}_{kl_1l_2}|_{\mathcal{F}_{ij}}$, such that (1) at this point, obstacles C_i and C_j are the closest obstacles and obstacles C_k, C_{l_1}, and C_{l_2} are the second closest, and (2) there exists a point, x, on the outer boundary where $d_{l_1}(x) = d_{l_2}(x)$. A link can be formed by tracing $\mathcal{SS}_{l_1l_2}|_{\mathcal{F}_{ij}}$, a second-order two-equidistant surjective surface constrained to a two-equidistant face, past a second-order meet point, $\mathcal{F}_{kl_1l_2}|_{\mathcal{F}_{ij}}$. By the Boundedness Assumption (Assumption 1) and Lemma 6, $\mathcal{SS}_{l_1l_2}|_{\mathcal{F}_{ij}}$ is guaranteed to be unbounded and therefore must intersect another boundary component of $\mathcal{F}_k|_{\mathcal{F}_{ij}}$.   □

This section demonstrated how arrangements of GVG edges and GVG^2 equidistant edges, by themselves, can yield a disconnected HGVG. Next, we introduced a procedure that either links the disconnected HGVG or states a weak assumption that precludes the possibility a disconnected HGVG could exist. The following section demonstrates how other GVG^2 edges can give rise to a disconnected HGVG and how to connect it.

7. Connectivity with Boundary and Occluding Periods

Boundary and occluding edges can also form periods that give rise to second-order generalized Voronoi regions with disconnected boundary components, and hence a disconnected HGVG. Both periods require the robot to perform gradient descent of the multiobject distance function constrained to a two-equidistant face to achieve linking. In fact, they rely on the property that the multiobject distance function has a unique minimum on a two-equidistant face, as described by the following proposition and lemma:

PROPOSITION 10.   The restriction of the multiobject distance function D to a k-equidistant face is smooth. That is, the generalized gradient of $D(x)$ projected onto $T_x \mathcal{F}_{i_1 \ldots i_k}$ is equal to $\pi_{T_x \mathcal{F}_{i_1 \ldots i_k}} \nabla d_i$ for all $i \in \{i_1 \ldots i_k\}$, where π is the orthogonal projection operator.

Let E be a plane in $T_x \mathbb{R}^m$. Let v_e be the unique minimum length vector in E (i.e., v_e is based at the origin of $T_x \mathbb{R}^m$ and its head is in E). Define P_E to be the subspace of $T_x \mathbb{R}^m$ parallel to E, i.e., $P_E = E - v_e$. Let $P_E^{\perp}$ be the orthogonal compliment of P_E. Therefore, $T_x \mathbb{R}^m = P_E \bigoplus P_E^{\perp}$ and thus for all vectors $u \in T_x \mathbb{R}^m$, u can be written as the sum $u_1 + u_2$ where $u_1 \in P_E$ and $u_2 \in P_E^{\perp}$. The orthogonal projection $\pi_{P_E}(u)$ is u_1. We can now define the orthogonal projection operator π_E to be π_{P_E}.

Proof.   Note that $\partial D(x)$ is the affine hull of the heads of the k gradient vectors $\nabla d_{i_1}, \ldots, \nabla d_{i_k}$. So, $\partial D(x)$ can be viewed as a plane in $T_x \mathbb{R}^m$. Transversality considerations imply that $\partial D(x)$ and $T_x \mathcal{SS}_{i_1 \ldots i_k}$ intersect at a point, and thus the generalized gradient of D constrained to $T_x \mathcal{SS}_{i_1 \ldots i_k}$ is always a point, not a vector. This point, which we denote by $v \in T_x \mathcal{SS}_{i_1 \ldots i_k} \bigcap \partial D(x)$, is the closest point in $\partial D(x)$ to $0 \in T_x \mathbb{R}^m$.

Define P to be a subspace of $T_x \mathbb{R}^m$ given by $P = \partial D(x) - v$ (again, $\partial D(x)$ is viewed as a plane). The orthogonal projection of $u \in \partial D(x)$ is given by

$$\pi_{T_x \mathcal{SS}_{i_1 \ldots i_k}} : \partial D(x) \to T_x \mathcal{SS}_{i_1 \ldots i_k}. \qquad (21)$$

Since D and $\pi_{T_x \mathcal{SS}_{i_1 \ldots i_k}}$ are continuous, the restriction of the generalized gradient of D on $\mathcal{SS}_{i_1 \ldots i_k}$ is continuous. Therefore, the restriction of the multiobject distance function D to a k-equidistant face is smooth. $\square$

LEMMA 13.   The multiobject distance function, restricted to a two-equidistant surjective surface of two convex obstacles, has one global minimum and no other extrema on the two-equidistant surjective surface. In other words, except at the global minimum, the generalized gradient of the multiobject distance function never projects to zero on any tangent space of a two-equidistant surjective surface.

Proof.   Let $\pi_{T_x \mathcal{SS}_{ij}}$ be the orthogonal projection operator onto $T_x \mathcal{SS}_{ij}$. Let l be the shortest distance between two convex obstacles C_i and C_j. Therefore, for all $x \in \mathcal{SS}_{ij}$, $D(x) > l$. Assume that there exists a point x where $\pi_{T_x \mathcal{SS}_{ij}} \partial D(x) = 0$. By hypothesis, $D(x) = L > l$. By Proposition 10, $\pi_{T_x \mathcal{SS}_{ij}} \nabla d_i(x) = \pi_{T_x \mathcal{SS}_{ij}} \nabla d_j(x) = 0$. That is, $\nabla d_i(x)$ and $\nabla d_j(x)$ are each orthogonal to $T_x \mathcal{SS}_{ij}$. In fact, by definition of the two-surjective equidistant surface, $\nabla d_i(x) = -\nabla d_j(x)$.

Let $HC_i(x)$ and $HC_j(x)$ be two supporting hyperplanes of C_i and C_j, respectively, such that they are orthogonal to $\nabla d_i(x)$ and $\nabla d_j(x)$, respectively, and pass through the nearest points in C_i and C_j to x, respectively (see Fig. 37).

Since $\nabla d_i(x) = -\nabla d_j(x)$, $HC_j(x)$ is orthogonal to $\nabla d_i(x)$ as well. Therefore, $HC_i(x)$ and $HC_j(x)$ are parallel. Thus, the distance between convex obstacles C_i and C_j can never be less than L, which is a contradiction. $\square$

With these two results, we can now develop linking strategies to boundary and occluding periods.

7.1. Boundary Periods

EXAMPLE 8.   In this example, we consider a variation of the environment in Figure 16. The box in the middle of the room has the same height as the room itself. A side view of the two-equidistant face defined by the box and the ceiling is depicted in Figure 38 and a top view in Figure 39.

A path from the GVG cycle to the boundary period can be determined by following the projection of the negated gradient onto the two-equidistant face.

LEMMA 14.   Boundary Link: In $\mathbb{R}^3$, if a boundary period exists on the boundary of the second-order generalized Voronoi region, then it must be an "inner boundary" and a link exists from the outer boundary to it.
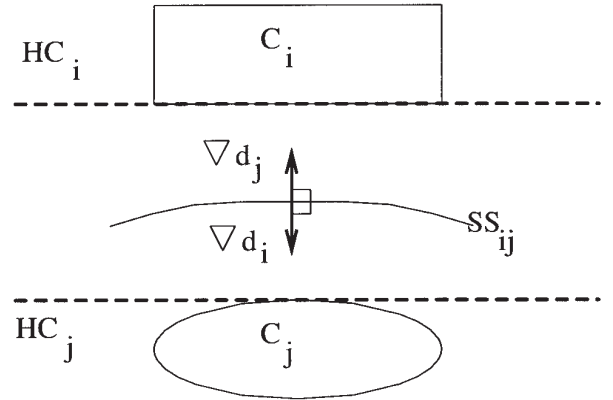

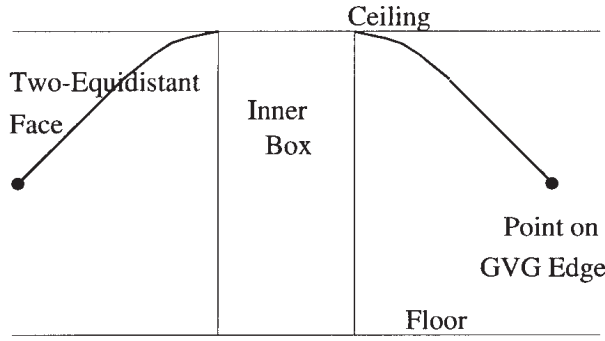Fig. 37. The supporting planes for convex obstacles C_i and C_j.

Fig. 38. The thick solid line represents a side view of the equidistant face defined by the box and the ceiling, and the solid dot delineates a point on the GVG cycle surrounding the box.
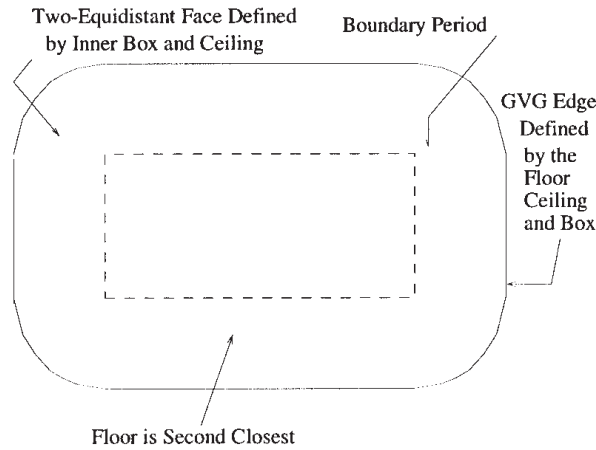

Fig. 39. Two-equidistant face between the box and the ceiling, as viewed from above, is drawn with a boundary period.

Proof. Proposition 10 states that the multiobject distance function, which is nominally not smooth, is smooth when it is constrained to a k-equidistant surjective surface (and thus a k-equidistant face).

Lemma 17 guarantees that a two-equidistant surjective surface, SS_{ij}, is unbounded. By hypothesis, it has only one boundary, C_{ij}. When C_{ij} is a Jordan curve, the bounded portion of SS_{ij} is the empty set, and the unbounded portion of SS_{ij} is SS_{ij}. Therefore, the generalized Voronoi region, $\mathcal{F}_k|_{\mathcal{F}_{ij}}$, which has C_{ij} on its boundary, lies in the unbounded portion of SS_{ij}. Therefore, C_{ij} is an inner boundary.

Lemma 17 and Proposition 10 guarantee that in the interior of the second-order generalized Voronoi region that has a boundary period, the projected generalized gradient of D never vanishes. Since $D(x) > 0$ for all $x \in$ interior$\mathcal{F}_k|_{\mathcal{F}_{ij}}$ and $D(x) = 0$ on the boundary period, gradient descent of D constrained to $\mathcal{F}_{ij}$ traces a path to the boundary period from any point in the second-order generalized Voronoi re-

gion. Therefore, a link can be made from the outer boundary to the boundary period via gradient descent of D. Similarly, the Boundedness Assumption (Assumption 1) guarantees that a link can be made from the boundary period to the outer boundary via gradient ascent of D. □

7.2. Occluding Period

EXAMPLE 9. Hole on top of box (continued): Recall the environment from Example 3, which is a rectangular enclosure with a box in its interior. On top of the box, there is an opening that could be a through-hole, an entrance to a subenvironment or a dimple. See Figures 16 and 17.

Since in this example we are only interested in the GVG edges associated with the box, Figure 40 contains only the box, the GVG structures associated with it (thick solid lines), and an occluding edge (thick dotted lines).

The GVG structure associated with the hole is connected to the occluding edge using GVG^2 equidistant edges. Using a linking procedure described later in Section 7, the outer GVG is linked to the occluding edge. The result is that the GVG is now connected through a link, an occluding edge, and a GVG^2 equidistant edge (see Fig. 41).

LEMMA 15. Occluding Link: In $\mathbb{R}^3$, if an occluding period exists on the boundary of a second-order generalized Voronoi region, then a link can be made to the period.

The proof of the above lemma is broken down into two cases: (1) when the global minimum of D constrained to the two-equidistant face is inside the occluding period (or on it), and (2) when the global minimum is outside the occluding period.

LEMMA 16. In $\mathbb{R}^3$, if the global minimum of D is contained inside of an occluding period, then gradient descent of D, constrained to the two-equidistant face, traces a path that is guaranteed to link the outer boundary of a second-order generalized Voronoi region to the occluding period.

Proof. Lemma 13 asserts that there is only one extremum of D, constrained to the two-equidistant face, and that extremum is the global minimum of D. Therefore, all paths that are traced out by gradient descent of D, constrained to the two-equidistant face, will terminate at the global minimum of D. Since the global minimum is inside (or on) the occluding period, such a path must traverse the occluding period. Therefore, gradient descent traces a path that brings the robot to an occluding period. □

When the projected gradient disappears, a more active approach is required. One option is an exhaustive search of the two-dimensional second-order generalized Voronoi region in which $\pi_{T_x \mathcal{F}_{ij}} \partial D(x)$ vanishes. Although this option may seem undesirable, it would only have to be invoked in a handful of small regions where the gradient goes to zero before arriving at an occluding period.
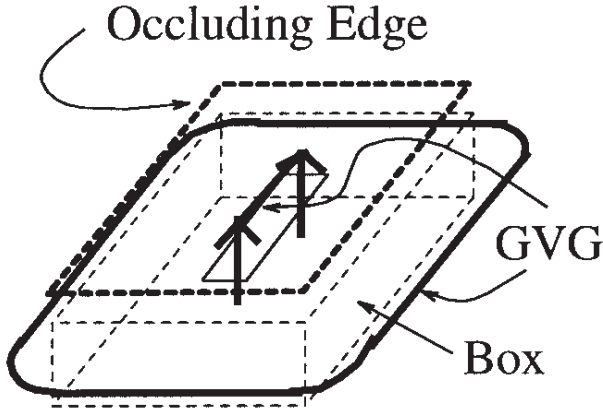
Occluding Edge

Fig. 40. The occluding edge, represented by a thick dotted line, is defined by the visible-distance function. The GVG is represented by the thick solid lines, and the inner box is drawn in thin dashed lines.
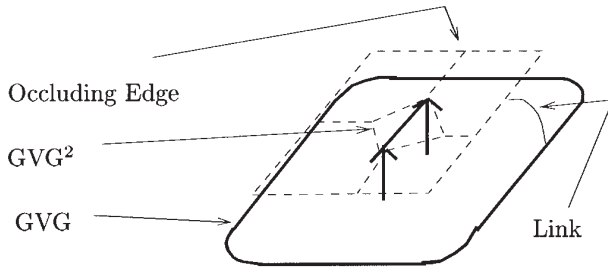

Fig. 41. The GVG surrounding the box is connected to the GVG associated with the hole through a link from the GVG surrounding the box to the occluding edge. The box is removed for clarity.

Fortunately, there exists an alternative method, whose rigorous proof is the topic of current work. Let $\mathcal{F}_{ij}$ be the two-equidistant face for C_i and C_j, and C_k be the second closest obstacle. Without loss of generality, assume that C_j occludes C_k. Let x be the point where $\pi_{T_x \mathcal{F}_{ij}} \partial D(x) = 0$. Let v be any vector that runs along a line that passes through x and C_k and is tangent to C_j.

In this approach, the robot again performs gradient descent of D. If it reaches the occluding period, then the procedure terminates with success. However, since the global minimum of D is outside of the occluding period, the robot did not reach the occluding period. In this case, starting from the global minimum of D, the robot moves in a path on $\mathcal{F}_{ij}$ in such a way that v and $\nabla d_k(x)$ converge on each other. In other words, the robot traces a path determined by $\nabla \langle -d_k(x), v \rangle$. When the vectors v and ∇d_k become collinear, the robot has arrived at a point on the occluding period.

Note that this method is not guaranteed to work but our experiments indicate that it works often. In fact, we have not found a counterexample yet. However, lack of existence of a counterexample does not serve as a proof. Therefore, when $\nabla \langle -d_k(x), v \rangle$ vanishes, the robot must perform an exhaustive search of the second-order generalized Voronoi region for the occluding period.

7.3. Exhaustive Search

In this section, we discuss connectivity when all assumptions are relaxed. Figure 42 contains a cross-section of a three-dimensional environment similar to the one found in Figure 15. In Figure 42, the floor is slanted and the inner obstacle is a sphere. The local minimum of D on $\mathcal{F}_{ij}$ is pointed out, and the shared region represents the set of points that are visible from this local minimum. Figure 43 contains the same environment, but the occluding period is drawn as a dotted line. The gray region is the set of points that are *not* visible from the occluding period.

The robot is guaranteed to travel along the occluding period and, if necessary, reach the local minimum. Unfortunately, the robot is still not guaranteed to become within line of sight of all structures by simply traveling along the occluding period and encountering the local minimum. The dark gray area in Figures 44 and 45 is the set of points on C_i that cannot be seen from both local minimum and the occluding period. The robot
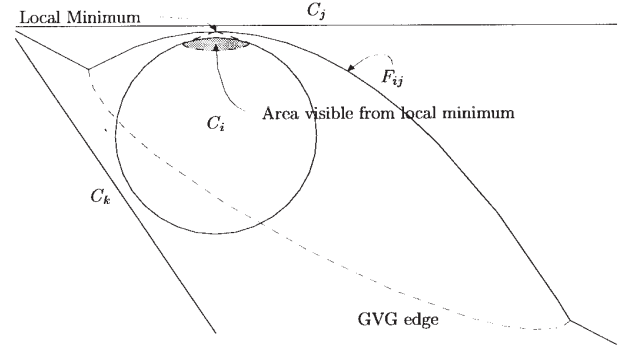

Fig. 42. Three-dimensional enclosure with a sphere floating in the middle of it. Local minimum and region visible from it are denoted.
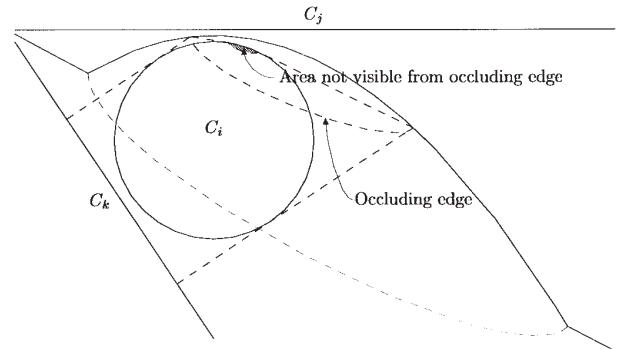

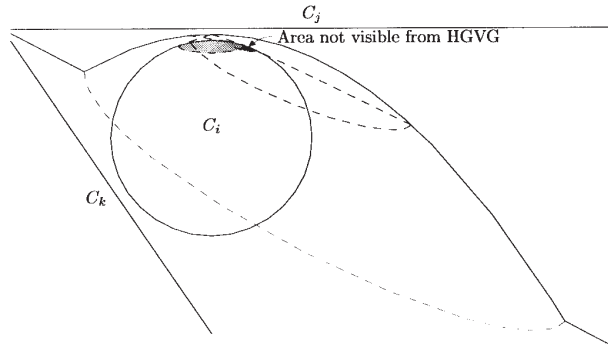Fig. 43. Occluding period and region not visible from it.

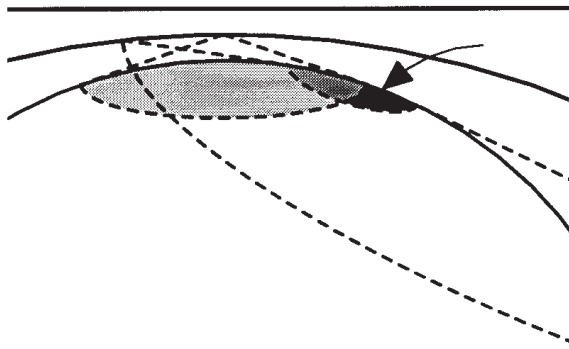Fig. 44. Region not visible from occluding period and local minimum.

Fig. 45. Close-up of region not visible from occluding period and local minimum.

may see this region when forming the link for the GVG cycle to the occluding period, but there is no guarantee. Therefore, in the general case, the robot needs to search this second-order generalized Voronoi region to find all roadmap fragments.

Other works in three-dimensional exploration have noted the problem that at some point, the planner requires some sort of exhaustive search. In Rimon and Canny (1994), Rimon points out that the robot requires some sort of active perception (i.e., active search) because critical points are not always guaranteed to be within line of sight of the roadmap fragment. However, there are no well-established thresholds or conditions that direct the robot to enter "active search" mode to find critical points. Moreover, Rimon's work does not identify which regions of space require the active search. Kutulakos, Dyer, and Lumelsky's (1994) approach to three-dimensional path planning in unknown environments also requires an exhaustive search of two-dimensional regions that correspond to the boundaries of the obstacles between the start and goal. This is not to say that three-dimensional exploration requires exhaustive search, but the current state-of-the-art in three-dimensional exploration requires exhaustive search of

subsets or patches of two-dimensional manifolds. The work presented in this paper identifies these subsets and prescribes a condition as to when to invoke the exhaustive search process. It should be noted, however, that for most of the environments we experimented with, the HGVG approach did not require exhaustive search of two-dimensional patches.

Figure 46 summarizes the search for occluding periods.

8. Conclusion

This paper introduces a new roadmap structure called the *hierarchical generalized Voronoi graph* (HGVG). The robot uses the HGVG by finding a path onto it (accessibility), traversing the HGVG to the vicinity of the goal (connectivity), and constructing a path from the HGVG to the goal (departability). Since a bulk of the planning occurs on the one-dimensional structure of a multidimensional configuration space or work space, the HGVG dramatically simplifies motion planning for robots operating in real environments.

To guarantee the appropriate dimension count, we introduce a transversality assumption, which essentially is a stability requirement on the placement of obstacles. This transversality assumption is a generalization of the general position assumptions, such as no four points can be co-circular, that are often made in Voronoi diagram literature.

To define the HGVG, we introduced a new distance function that relies solely on line-of-sight information. This is particularly important for sensor-based construction of the
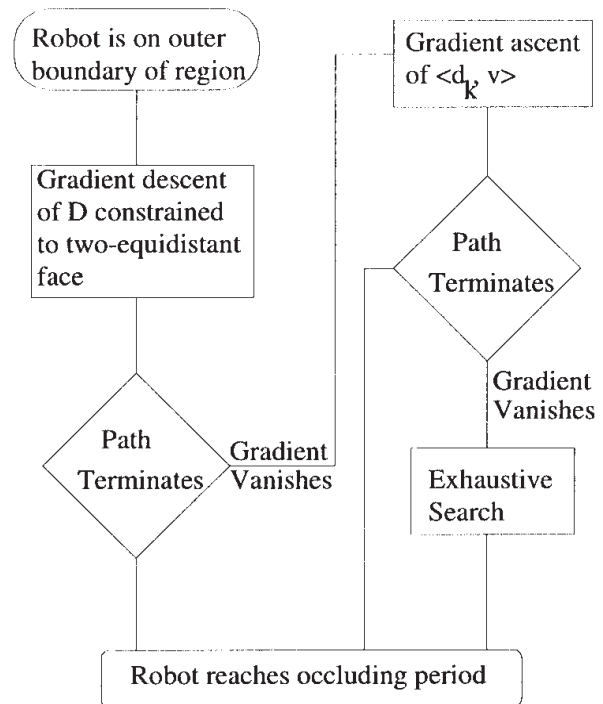

Fig. 46. Flow Chart.

HGVG, as sensors can only provide line-of-sight information. This distance-based definition also allows HGVG to handle concave obstacles, whereas traditional geometric structures and algorithms are limited to convex obstacles. Essentially, the HGVG definitions require a surjectivity condition from the preimage theorem, which is ensured when obstacles are locally convex. Finally, the definition and construction procedure of the HGVG do not require the obstacles to be polyhedra, which is an assumption often made with most complete algorithms.

Using some results from nonsmooth analysis, we demonstrate that the HGVG roadmap has the property of accessibility in a bounded subset of an m-dimensional Euclidean space. When full knowledge of the world is available, then departability reduces to accessibility in reverse and, thus, the HGVG has departability. However, when the robot is searching for the goal, a reverse-accessibility procedure cannot serve as a departability method. Incremental departability is described in the companion paper.

A bulk of this paper examined connectivity of the HGVG. First, the GVG (a subset of the HGVG) is shown to be connected when an assumption supplied by Yap is upheld. Unfortunately, this assumption was too restrictive, so it was relaxed and connectivity of the HGVG in $\mathbb{R}^3$ was considered next. Under a certain set of weak assumptions, the HGVG was shown to be connected. These assumptions essentially required the environment to be cluttered and are thus reasonable for many applications, such as those that require highly articulated robots.

Finally, connectivity was examined when all assumptions were relaxed. In this scenario, the robot has to perform an active search on some subsets of two-dimensional manifolds to ensure connectivity. Other three-dimensional path-planning techniques in unknown environments also require an active search phase. The HGVG approach supplies conditions of when to search and localizes where to search, whereas other methods do not afford these conditions. Future work will consider how to efficiently search these two-dimensional sheets without having to exhaustively search them.

Our ultimate goal is to enable highly articulated sensor-equipped robots to explore unknown environments by constructing roadmaps. Instead of generalizing the connectivity result for a point in an m-dimensional configuration space, future work will include defining a roadmap for a robot modeled as a line segment, sometimes called a *rod*, operating in a three-dimensional environment. The roadmap will be based on the distance between a rod and an object. The next step is to extend the results of the rod roadmap to that of a convex set, which in turn will be extended to the development of a roadmap for a chain of convex sets that model a highly articulated robot. We chose this point-rod-blob-snake approach because sensors directly provide work space distance information but not configuration space distances. Furthermore, we believe error analysis on work space distance measure-

ments to be more tractable than error analysis on configuration space distance measurements.

We make no claim that the HGVG has any clear advantage over other methods for classical motion planning, but since distance functions define the HGVG, a sensor-based planner can easily construct it. Once a robot constructs the HGVG, it has in essence explored the environment because the robot can use the HGVG for future excursions. A companion paper (Choset and Burdick 2000) describes the sensor-based construction procedure when the robot has no prior information about the environment.

Appendix A: Boundary Edge and Floating Boundary Edge

EXAMPLE 10. Hole: The room depicted in Figure 47 contains a hole or duct in one of its side walls. The bottom and front faces of the duct are labeled C_i and C_j, respectively. Note also that the duct enters the room at a height greater than half the distance between the floor and ceiling.

Consider the two-equidistant face defined by the duct's front and bottom faces, C_i and C_j. The shaded region in Figure 48 is a portion of a two-equidistant surface, $\mathcal{S}_{ij}$, defined by objects C_i and C_j. The boundary of the shaded region is dotted to emphasize that it is unbounded (i.e., a sphere of finite radius cannot contain the two-equidistant surface).

Recall that a two-equidistant surjective surface is the set of points in a two-equidistant surface such that the gradients to each defining obstacle do not coincide. The shaded region in Figure 49 is a portion of the two-equidistant surjective surface, $\mathcal{SS}_{ij}$, defined by C_i and C_j. Note that this region is unbounded. Figure 50 illustrates the side view of Figure 49, where the solid line represents the unbounded $\mathcal{SS}_{ij}$. The float-
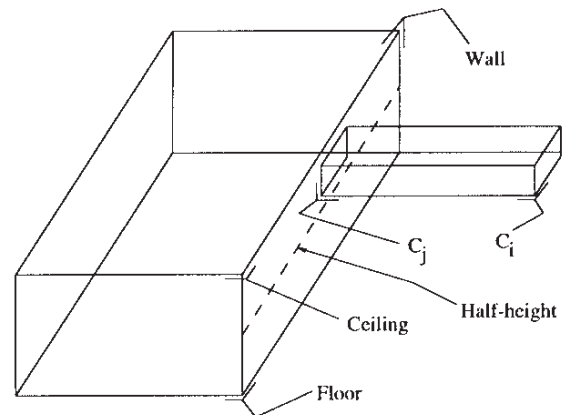

Fig. 47. A room with a hole in its side wall. The dotted line marks the half-height of the room.
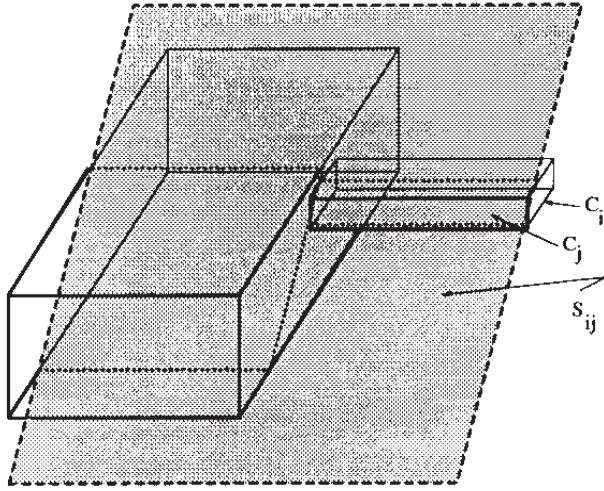
Fig. 48. The shaded region is S_{ij}. It is bordered by thick dashed lines to emphasize that S_{ij} is unbounded. The thick dotted lines correspond to points where S_{ij} intersects the rectangular enclosures. The thick solid lines on the rectangular enclosures are drawn to emphasize the features on the enclosure that are in front of S_{ij} in this view.
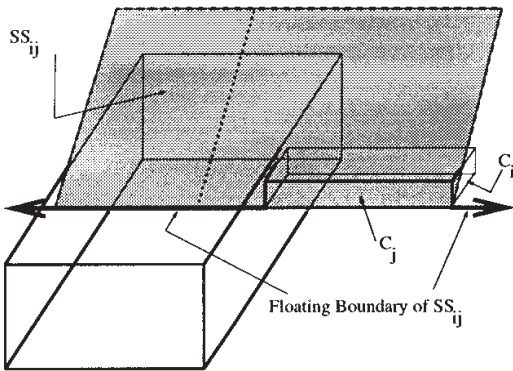

Fig. 49. The shaded region SS_{ij}, which is also unbounded. The thick double-arrowed line represents the boundary of SS_{ij}, which is also unbounded. The dotted line simply represents a path in SS_{ij}.

ing boundary surface (solid line, Fig. 49) is the portion of boundary of the two-equidistant surjective surface where the two distance function gradient vectors coincide.

The shaded region in Figure 51 depicts the two-equidistant face, $\mathcal{F}_{ij}$, which is bounded. The boundary of $\mathcal{F}_{ij}$ consists of three parts: a GVG edge, a boundary edge, and a floating boundary edge. The boundary edge runs along the intersection of the boundaries of obstacles C_i and C_j. $D(x)$ is zero
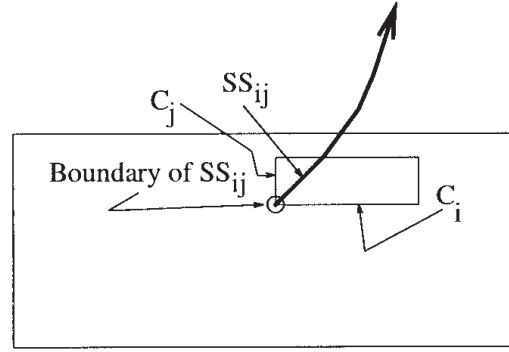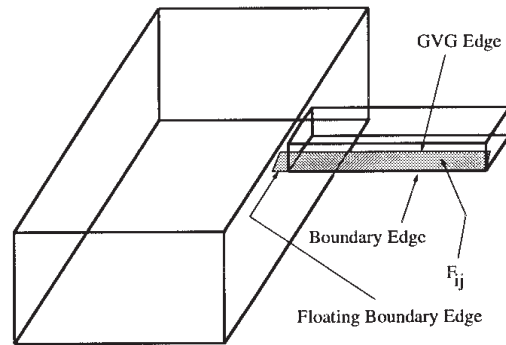

Fig. 50. SS_{ij} (Side view).

Fig. 51. $\mathcal{F}_{ij}$.

for all points on this portion of $\mathcal{F}_{ij}$. The floating boundary edge is the set of points in $\mathcal{F}_{ij}$, where $D(x)$ is greater than zero but $\nabla d_i(x) = \nabla d_j(x)$. The nearest point to all points on the floating boundary edge is a corner of the duct entrance.

Appendix B: Proofs of Lemmas in Section 6

Properties of Equidistant Surjective Surfaces

This section demonstrates two properties of equidistant surjective surfaces: (1) for k intersecting convex obstacles, they are unbounded, and (2) a two-equidistant face $\mathcal{F}_{ij}$ separates $\mathcal{FS}$ into two connected regions: one whose points are closer to C_i and the other whose points are closer to C_j.

LEMMA 17.   If the objects $C_{i_1} \ldots, C_{i_k}$ intersect, then the associated k-equidistant surjective surface, $SS_{i_1 \ldots i_k}$, is unbounded. In fact, if objects $C_{i_1}, \ldots, C_{i_k}$ intersect, then none of the gradients, $\nabla d_{i_1}(x), \ldots, \nabla d_{i_k}(x)$, is orthogonal to $T_x SS_{i_1 \ldots i_k}$ for all $x \in SS_{i_1 \ldots i_k}$. In other words, there are no extrema of D in the interior of $SS_{i_1 \ldots i_k}$.

Proof.   Assume that there exists an $x \in SS_{i_1 \ldots i_k}$ for which $\nabla d_{i_1}(x)$ is orthogonal to $T_x SS_{i_1 \ldots i_k}$. By Proposition 10,

$\nabla d_{i_j}(x)$ must be orthogonal to $T_x SS_{i_1...i_k}$ for all $j = 2, \ldots, k$ because $\nabla d_{i_1}(x)$ is orthogonal to $T_x SS_{i_1...i_k}$.

Let $HC_{i_1}(x)$ be the hyperplane that is orthogonal to ∇d_{i_1} and tangent to the nearest point, c_{i_1} in C_{i_1} to x. Since C_{i_1} is a convex set, C_{i_1} lies entirely on one side of $HC_{i_1}(x)$. Let $HC_{i_j}(x)$ be the hyperplanes similarly defined as above for $j = 2, \ldots, k$.

In $\mathbb{R}^m$, let S be an $(m-1)$-dimensional sphere centered at x with radius $D(x)$. By Assumption 2, the k closest points on the k closest obstacles form a $(k-1)$-dimensional hyperplane orthogonal to $T_x SS_{i_1...i_k}$ and passing through x. For $k > 2$, these k points define a $(k-2)$-dimensional sphere, termed a *subsphere* (S_{sub}), which is a subset of S and has a radius less than or equal to $D(x)$. When the radius of S_{sub} is equal to the radius of S, we say that S_{sub} is a *major subsphere* of S. For $j = 1, \ldots, k$, HC_{i_j} is tangent to S and passes through a point on the $(k-2)$-dimensional subsphere, S_{sub}.

Next, it needs to be shown that $HC_{i_1}, \ldots, HC_{i_k}$ cannot intersect at a point. We first show this when $k = 2$. The sphere S has co-dimension one. If ∇d_{i_1} and ∇d_{i_2} are orthogonal to $T_x SS_{i_1 i_2}$, then there are only two points (at opposite poles of the sphere) where the separating planes are tangent to S. In this case, the separating planes are parallel to each other (Fig. 37). By definition of a convex set, if the separating planes never intersect, then the obstacles cannot intersect. This is a contradiction. Therefore, for $k = 2$, no gradient vector can be orthogonal to $T_x SS_{i_1...i_k}$, and thus $\partial D(x)$ has no local maxima. Since $\partial D(x)$ has no local maxima, it has no global maxima and thus $SS_{i_1...i_k}$ is unbounded.

In general, if the gradients $\nabla d_{i_1}(x), \ldots, \nabla d_{i_k}(x)$ are orthogonal to $T_x SS_{i_1...i_k}$, then S_{sub} and S have the same radius. In other words, S_{sub} is a major subsphere. It can be shown that if k hyperplanes are tangent to S at a point in S_{sub}, then they can never intersect at a point. Since $HC_{i_1}, \ldots, HC_{i_k}$ can never intersect at a point, the obstacles $C_{i_1}, \ldots, C_{i_k}$ cannot intersect at a point either. This is a contradiction, and thus $SS_{i_1...i_k}$ is unbounded. $\square$

LEMMA 18.   A two-equidistant surjective surface for two disjoint convex sets is an unbounded separator in $\mathcal{W}$.

Proof. Let SS_{ij} be a two-equidistant surface for obstacles C_i and C_j in the space $\mathcal{W}\backslash(\bigcup_{h \neq i,j} C_h)$. Let S_i be the set of points in $\mathcal{W}\backslash(\bigcup_{h \neq i,j} C_h)$ closer to C_i than C_j. Define S_j similarly. That is,

$$S_i = \{x \in \mathcal{W}\backslash(\bigcup_{h \neq i,j} C_h) : d_i(x) \leq d_j(x)\}$$

$$S_j = \{x \in \mathcal{W}\backslash(\bigcup_{h \neq i,j} C_h) : d_j(x) \leq d_i(x)\}. \quad (22)$$

The two-equidistant surjective surface, SS_{ij}, is on the boundary of both S_i and S_j.

Let F_i^t be the flow of ∇d_i and let $SS_i = \{x \in S_i : F_i^t \in SS_{ij}$ for some $t\}$. Define SS_j similarly.

The mapping $F_i : \mathbb{R} \times S_i \rightarrow \mathcal{W}\backslash C_i$ is a continuous mapping. Let $Q_i = F^{-1}(SS_{ij})$. Q_i is closed because it is the preimage of a closed set under a continuous mapping. Note that $(t, x) \in Q_i$ if and only if $F_i^t(x) \in SS_{ij}$. (So, $x \in SS_{ij}$ implies that $(0, x) \in Q_i$.)

Since SS_{ij} is the image of a connected set under a continuous mapping F_i, SS_{ij} is connected. Therefore, S_i and S_j share a common connected boundary: SS_{ij}. This boundary separates $\mathcal{W}$ into two regions: points closer to C_i and points closer to C_j. Since S_i and S_j are both unbounded, so must be SS_{ij}.

$\square$

Proof of Lemma 8

LEMMA 8.   If the three-equidistant face $\mathcal{F}_{ijk}$ is not empty, then the second-order generalized Voronoi region $\mathcal{F}_k|_{\mathcal{F}_{ij}}$ must not be empty. Furthermore, if $\mathcal{F}_{ijk} \neq \emptyset$, then $\mathcal{F}_{ijk} \subset \mathcal{F}_k|_{\mathcal{F}_{ij}}$.

Proof. Pick $x \in \text{interior}(\mathcal{F}_{ijk})$. By definition, $d_i(x) = d_j(x) = d_k(x) < d_h(x)$ for all $h \neq i, j, k$. For a nbhd(x), let $Y(x) = \text{nbhd}(x) \bigcap (\text{interior}(\mathcal{F}_{ij})\backslash\text{interior}(\mathcal{F}_{ijk}))$. By definition, $d_i(y) = d_j(y) < d_k(y)$ for all $y \in Y(x)$. By continuity of the single object distance function, for all $h \neq i, j, k$, $d_k(y) < d_h(y)$ for all $y \in Y(x)$. Therefore, for all $y \in Y(x)$, $d_i(y) = d_j(y) < d_k(y) < d_h(y)$ for all $h \neq i, j, k$.

Therefore, there exists a region where C_i and C_j are the closest obstacles and C_k is the second closest. That is, $\mathcal{F}_k|_{\mathcal{F}_{ij}} \neq \emptyset$. Furthermore, $\mathcal{F}_{ijk}$ is a subset of $\partial \mathcal{F}_k|_{\mathcal{F}_{ij}}$ because

$$\begin{aligned} \mathcal{F}_{ijk} \;&= \{x : \forall h\, d_h(x) \geq d_i(x) = d_j(x) = d_k(x)\} \\ &\subset \partial\{x : \forall h\, d(h) \geq d_k(x) \geq d_j(x) = d_i(x)\} \\ &= \partial \mathcal{F}_k|_{\mathcal{F}_{ij}}, d_k(x) = d_i(x) = d_j(x)\}. \end{aligned}$$

where ∂ is the boundary operator.

Therefore, by definition, if $\mathcal{F}_{ijk} \neq \emptyset$, then it is a nonempty subset of the boundary of $\mathcal{F}_k|_{\mathcal{F}_{ij}}$. $\square$

Proof of Lemma 9

LEMMA 9   The boundary of a second-order generalized Voronoi region contains at most *one* three-equidistant face. That is, $\mathcal{F}_{pqr} \subsetneq \mathcal{F}_k|_{\mathcal{F}_{ij}}$ for all $\{p, q, r\} \neq \{i, j, k\}$.

Proof. Assume that $\mathcal{F}_{ijk}$ and $\mathcal{F}_{ijl}$ are on the boundary of $\mathcal{F}_k|_{\mathcal{F}_{ij}}$. By definition, for all $x \in \mathcal{F}_k|_{\mathcal{F}_{ij}}$, it must be true that $d_l(x) \geq d_k(x) \geq d_i(x) = d_j(x)$ for all $l \neq i, j, k$. Since $\mathcal{F}_{ijl} \subset \mathcal{F}_k|_{\mathcal{F}_{ij}}$ (by assumption), for all $x \in \mathcal{F}_{ijl}$, $d_k(x) \leq d_l(x)$. Thus, for all $x \in \mathcal{F}_{ijl}\backslash\mathcal{F}_{ijk}$ (which is a subset of $\mathcal{F}_k|_{\mathcal{F}_{ij}}$), $d_k(x) \leq d_l(x)$. However, this is a contradiction because for all $x \in \mathcal{F}_{ijl}\backslash\mathcal{F}_{ijk}$, $d_l(x) < d_k(x)$. $\square$

Proof of Lemma 4

LEMMA 4.   When equidistant faces intersect transversally (Assumption 2 is upheld), a GVG cycle cannot contain a meet point.

Let $\mathcal{F}_{ijk}$ be the GVG edge equidistant to obstacles C_i, C_j, and C_k. Assume there is an object C_l positioned such that $x \in \mathcal{F}_{ijk}$ is a point where $d_i(x) = d_l(x)$. By Proposition 1, the GVG edge $\mathcal{F}_{ijl} \neq \emptyset$ and it intersects $\mathcal{F}_{ijk}$ at x. By definition of the surjective equidistant surfaces, SS_{ijk} and SS_{ijl} also intersect at x. The three-equidistant surjective surface SS_{ijl} must tangentially intersect SS_{ijk} because $\mathcal{F}_{ijk}$ is a cycle. Such an intersection is nontransversal, which cannot occur when Assumption 2 is in effect. Therefore, there cannot be an object C_l positioned such that there is a point $x \in \mathcal{F}_{ijk}$ such that $d_i(x) = d_l(x)$, and hence a GVG cycle cannot contain any meet points.

Proof of Lemma 5

LEMMA 5.   A GVG cycle cannot contain any boundary or floating boundary points.

Proof.   Let $\mathcal{F}_{ijk}$ be a GVG edge equidistant to objects C_i, C_j, and C_k. Since the GVG edge is a cycle, it is bounded and, thus, there exists a point x^* such that $D(x^*) > D(x)$ for all $x \in \mathcal{F}_{ijk}$. At x^*, $\nabla d_i(x)$ is orthogonal to $T_{x^*}\mathcal{F}_{ijk}$.

Now the proof follows by contradiction. Assume there is a point where $D(x) = 0$. That is, C_i, C_j, and C_k intersect to form a boundary point. By Lemma 17, introduced earlier, there cannot be a point where $\nabla d_i(x)$ is orthogonal to $T_x\mathcal{F}_{ijk}$. This, however, is a contradiction, and thus there cannot be a point on a GVG cycle where $D(x) = 0$.

A similar argument can be made for floating boundary points. □

Proof of Lemma 6

LEMMA 6.   In $\mathbb{R}^3$, a three-equidistant surface, SS_{ijk}, is either C^2-diffeomorphic to S^1 (i.e., it is a GVG cycle) or it is unbounded.

Proof.   First, we show the case when C_i, C_j, and C_k are disjoint convex sets and then we show the case when they overlap. By Lemma 18, a two-equidistant surjective surface for two disjoint convex sets is a separator in $\mathcal{W}$.

By a similar argument, it can be shown that SS_{ijk} is a separator on SS_{ij}. In $\mathbb{R}^3$, the preimage theorem asserts that SS_{ijk} is one-dimensional. By the Jordan curve lemma, SS_{ijk} in $\mathbb{R}^3$ can either be (1) a manifold C^2-diffeomorphic to S^1 or (2) an unbounded manifold C^2-diffeomorphic to $\mathbb{R}$.

Now, we consider the case where the obstacles, C_i, C_j, and C_k, intersect to form a boundary point, C_{ijk}, out of which SS_{ijk} emanates. Lemma 17 asserts that SS_{ijk} is unbounded. □

Proof of Lemma 7

LEMMA 7.   A GVG^2 equidistant edge can only intersect the GVG at a meet point.

Proof.   Consider the GVG^2 equidistant edge $\mathcal{F}_{kl}|_{\mathcal{F}_{ij}}$. For all points $x \in \mathcal{F}_{kl}|_{\mathcal{F}_{ij}}$, $d_k(x) = d_l(x) \geq d_i(x) = d_j(x)$. When $d_i(x) = d_j(x) = d_k(x)$ for some $x \in \mathcal{F}_{kl}|_{\mathcal{F}_{ij}}$, $d_i(x) = d_j(x) = d_k(x) = d_l(x)$. However, x cannot be in the interior of a generalized Voronoi edge $\mathcal{F}_{ijk}$ because for all $y \in \mathrm{interior}(\mathcal{F}_{ijk})$, $d_i(y) = d_j(y) = d_k(y) < d_h(y)$ for all h. □

References

Abraham, R., Marsden, J. E., and Ratiu, T. 1988. *Manifolds, Tensor Analysis, and Applications.* 2d ed. New York: Springer-Verlag.

Aurenhammer, F. 1991. Voronoi diagrams—A survey of a fundamental geometric structure. *ACM Computing Surveys* 23:345–405.

Avis, D., and Bhattacharya, B. K. 1983. Algorithms for computing D-dimensional Voronoi diagrams and their duals. *Advances in Computing Research* 1:159–180.

Brooks, R. A. 1986. A robust layered control system for a mobile robot. *IEEE Journal on Robotics and Automation* RA-2(March).

Canny, J. F. 1988. *The Complexity of Robot Motion Planning.* Cambridge, MA: MIT Press.

Canny, J. F., and Lin, M. C. 1993. An opportunistic global path planner. *Algorithmica* 10:102–120.

Choset, H. 1998. Nonsmooth analysis, convex analysis, and their applications to motion planning. Special issue of *Int. J. Comp. Geom. and Apps.* To appear.

Choset, H., and Burdick, J. 2000. Sensor based exploration: Incremental construction of the hierarchical generalized Voronoi graph. *International Journal of Robotics Research* 19:96–118.

Choset, H., and Burdick, J. W. 1994. Sensor based planning and nonsmooth analysis. *Proc. IEEE Int. Conf. on Robotics and Automation*, San Diego, CA, pp. 3034–3041.

Choset, Howie. 1996. Sensor based motion planning: The hierarchical generalized Voronoi graph. Ph.D. thesis, California Institute of Technology, Pasadena.

Clarke, F. H. 1990. *Optimization and Nonsmooth Analysis.* Philadelphia, PA: Society of Industrial and Applied Mathematics.

Gat, E., and Dorais, G. 1994 (May). Robot Navigation by Conditional Sequencing. *Proc. IEEE Int. Conf. on Robotics and Automation*, San Diego, CA, pp. 1293–1299.

Kutulakos, K. N., Dyer, C. R., and Lumelsky, V. J. 1994 (May). Provable strategies for vision-guided exploration in three dimensions. *IEEE Int. Conf. on Robotics and Automation*, San Diego, CA.

Latombe, J. C. 1991. *Robot Motion Planning*. Boston, MA: Kluwer Academic.

Lumelsky, V., and Stepanov, A. 1987. Path planning strategies for point mobile automaton moving amidst unknown obstacles of arbitrary shape. *Algorithmica* 2:403–430.

Ó'Dúnlaing, C., and Yap, C. K. 1985. A "retraction" method for planning the motion of a disc. *Algorithmica* 6:104–111.

Rao, N.S.V., Kareti, S., Shi, W., and Iyenagar, S. S. 1993. Robot navigation in unknown terrains: Introductory survey of non-heuristic algorithms. *Oak Ridge National Laboratory Technical Report* ORNL/TM-12410(July):1–58.

Rao, N.S.V., Stolzfus, N., and Iyengar, S. S. 1991. A retraction method for learned navigation in unknown terrains for a circular robot. *IEEE Transactions on Robotics and Automation* 7(October):699–707.

Rimon, E., and Canny, J. F. 1994. Construction of C-space roadmaps using local sensory data—What should the sensors look for? *Proc. IEEE Int. Conf. on Robotics and Automation*, San Diego, CA, pp. 117–124.

Rowat, P. F. 1979. Representing the spatial experience and solving spatial problems in a simulated robot environment. Ph.D. thesis, University of British Columbia.

Scheimberg, S., and Oliveira, P. R. 1992. Descent algorithm for a class of convex nondifferentiable functions. *Journal of Optimization Theory and Applications* 72(February):269–297.

Schwartz, J. T., and Yap, C. K., eds. 1987. *Advances in Robotics: Algorithmic and Geometric Aspects of Robotics*. Vol. 1. Hillsdale, NJ: Lawrence Erlbaum.